Available online at www.sciencedirect.com
ScienceDirect
Journal of Catalysis 245 (2007) 91–109
JOURNAL OF CATALYSIS
www.elsevier.com/locate/jcat

# Mechanisms and rate laws for oxygen exchange on mixed-conducting oxide surfaces

S.B. Adler *, X.Y. Chen, J.R. Wilson

*Chemical Engineering Department, University of Washington, Box 351750, Seattle, WA 98195-1750, USA*

Received 13 July 2006; revised 15 September 2006; accepted 19 September 2006

Available online 27 October 2006

**Abstract**

Transition metal oxides with mobile electrons and oxygen ions (mixed conductors) constitute a broad class of materials that include selective oxidation catalysts, high-temperature electrocatalysts, and ion-transport membrane materials. Although the thermodynamic and transport properties of mixed conductors are generally understood, a consensus has not yet emerged regarding the mechanisms and rate laws governing exchange of oxygen with the bulk at the gas-exposed surface. To aid interpretation of existing kinetic data, and generate testable hypotheses for further research, this paper outlines a framework for predicting $O_2$ reduction rate laws based on specific reaction mechanisms. Based on nonequilibrium thermodynamics and transition state theory, this framework yields rate laws that are rigorously consistent with thermodynamics, yet allow rates of individual steps to be developed in terms of simple mass action laws, where appropriate. This framework is used to reexamine equilibrium oxygen-exchange kinetics reported for electron-rich perovskite mixed conductors $La_{1-x}Sr_xCoO_{3-\delta}$ (LSC) and $La_{1-x}Sr_xFeO_{3-\delta}$ (LSF), which have a metallic and a semiconducting band structure, respectively. Our analysis suggests that metallic band structure may play an important role in catalysis by stabilizing physisorbed $O_2$ on the surface. We also show that equilibrium surface exchange rates (as measured by $^{18}O/^{16}O$ isotopes, concentration steps, impedance, etc.) are generally only weak indicators of mechanism, and emphasize the need for kinetic data involving moderate to large displacements from equilibrium.


*Keywords:* Oxygen; Reduction; Mixed conductor; Oxide; Catalyst; Electrocatalysis; Solid oxide fuel cell; Cathode; Perovskite; Vacancy; Mechanism; Rate law

## 1. Introduction

Transition metal oxides with both mobile electrons and oxygen ions (mixed conductors) constitute a broad class of materials that include selective oxidation catalysts, ion-transport membrane materials, and high-temperature electrocatalysts for solid oxide fuel cells or solid-oxide electrolysis. An important feature of these materials is their ability to reversibly absorb and desorb oxygen into the lattice by continuous changes in oxidation state, without changes in overall bulk crystal structure. The rate of absorption/desorption is governed by bulk anion and electron transport, as well as catalytic reduction/oxidation of $O_2$ or other oxygen-containing molecules at the surface [1].

Although the thermodynamic and transport properties of mixed conductors are generally understood, a consensus has not yet emerged regarding the likely mechanisms or appropriate rate laws governing surface reactions. Of particular interest is $O_2$ reduction/oxidation, as illustrated in Fig. 1. Although numerous methods have been developed to measure and describe this reaction [2–8], a rigorous framework for connecting kinetic measurements to specific mechanisms has not yet emerged. One challenge in developing such a framework is that these materials are often highly doped or defective, leading to nonideal thermodynamic behavior. This precludes the use of simple mass action rate expressions, because these do not properly describe the thermodynamics in the limit of equilibrium. Of particular difficulty is the handling of mobile electronic species (electrons and holes) when materials fall somewhere between semiconductor and metal. As electrons become increasingly itinerant, they tend toward fixed entropy but vary in energy with electron occupation [9]. Thus mass action laws (which assume fixed energy but configurational entropy scaling as the logarithm of concentration) are expected to break down.

* Corresponding author.
*E-mail address:* stuadler@u.washington.edu (S.B. Adler).

0021-9517/$ – see front matter 
doi:10.1016/j.jcat.2006.09.019

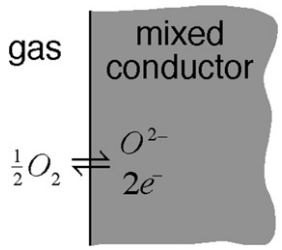


Fig. 1. Reversible oxygen exchange $\frac{1}{2}O_2^{(gas)} + 2e^{-(solid)} \rightleftarrows O^{2-(solid)}$ between a mixed conductor of variable oxidation state and the surrounding gas atmosphere.

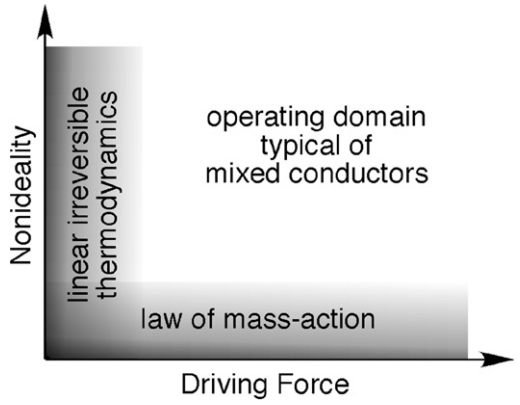


Fig. 2. Domains of validity for existing kinetic modeling approaches, expressed on a map of increasing departure from ideality vs magnitude of the thermodynamic driving force. Shading indicates increasing validity. Figure is based on that in Ref. [12].

Maier, who has extensively investigated the relationship between thermodynamics and kinetics in mixed conductors [10,11], has described the problem of nonideal thermodynamics as shown in Fig. 2 [12]. For ideal systems in which species free energy scales negatively with configurational entropy (e.g., lattice gas), a mass action rate expression can be used with no conflict with thermodynamics, even at high driving forces. This is often the case for gas-phase and surface catalytic reactions, leading to the widespread use of mass action rate expressions in heterogeneous catalysis (e.g., Langmuir–Hinshelwood kinetics). A mass action approach is also the norm in handling rate laws involving ideal point defects in solids [11]. In contrast, for nonideal systems, one can always develop a rate expression based on linear irreversible thermodynamics that is valid for small displacements from equilibrium. For example, Maier has used this approach to differentiate the expected linear force-flux coefficients governing various oxygen-exchange measurements [10]. This leaves a wide range of possible operating conditions involving both nonideal thermodynamics as well as large (nonlinear) driving forces. This regime is of particular interest in catalysis, where we often seek to apply nonlinear driving forces to probe mechanism, for example, to determine reaction order with respect to a particular species.

The proper means of incorporating nonideal thermodynamics into kinetic rate laws is a well-established subject of investigation [13,14]. In general, workers have approached this problem from the perspective of two asymptotic limits. For electrochemical (faradaic) reactions at solution–metal interfaces, the driving force is often purely *energetic*; that is, ions and electrons remain in fixed concentration but experience shifts in free energy relative to equilibrium due to changes in solution potential relative to the electrode [14]. In this scenario, any additional nonideal energetic interactions (e.g., solution thermodynamics) are often lumped together with kinetic parameters into a constant exchange current density (e.g., Butler–Volmer equation) [15]. Such a rate expression is thermodynamically rigorous at high driving forces, provided that solution composition remains fixed. Although mass action laws still are often used to estimate the composition dependence of the exchange current density, this approximation does not limit the thermodynamic rigor of the rate expression.

In contrast, the driving force for chemical reactions is inherently *entropic*, involving a displacement of species concentrations from equilibrium. In this case the role of nonideal energetic interactions is to modify species activity from ideality, resulting in departures from the law of mass action. Workers have generally found experimentally that rates scale with the concentration (not the activity) of the transition state species [16]. In this limit, driving force-dependent rate coefficients may be derived that incorporate the ratio of the activity coefficients of the reactants to that of the transition state. Examples include systems involving dilute strong electrolytes [13], strong species–solvent interactions [17,18], or high gas pressures [19]. This approach is ideally suited to systems in which all species (including the transition state) are molecular entities, whose excess free energy can be defined in terms of specific energetic interactions with their surroundings.

In the case of the $O_2$-exchange reaction (Fig. 1), one can identify similarities with both electrochemical and chemical reactions. The prevailing thermodynamics involve molecular species in the gas and on the surface, as well as ionic and electronic species on the surface and in the bulk. The reaction is nonfaradaic yet involves charged species that must cross a space charge region within the bulk material as if it were a solution. The rate may be coupled to molecular diffusion and surface transport processes, as well as to bulk ionic and electron transport. Thus to address this system adequately, we must take a step back and reconsider the nature of the driving force in this class of reactions. Doing so requires incorporating ideas from nonequilbrium thermodynamics, transition state theory, chemical kinetics, electrochemical kinetics, point defect theory, and band theory.

In what follows, we use a framework for treating reactions where the driving force explicitly involves both energetic and configurational entropic contributions. This approach begins by identifying the specific energetic and entropic contributions to the free energy for each reactant species. After separating the configurational entropy, the rate law can then be developed in a standard nonequilibrium thermodynamic form, with mass action expressed explicitly where appropriate. This framework is used to predict the kinetics of $O_2$ exchange on mixed conducting oxides with high concentrations of free electron carriers. Scenarios considered include metallic versus semiconducting band structure, as well as various possible rate-

limiting steps. These models are then used to reexamine the equilibrium exchange rates on the perovskite mixed conductors $La_{1-x}Sr_xCoO_{3-\delta}$ (LSC) and $La_{1-x}Sr_xFeO_{3-\delta}$ (LSF).

## 2. Oxygen exchange kinetics for mixed conductors with metallic versus semiconducting band structure

### 2.1. A general form for kinetic rate expressions based on thermodynamic driving forces

As explained in Appendix A, the net rate of any elementary reaction step ($j$) obeying transition state theory can be stated in the form

$$r_j = k_j e^{-\Delta G^0_{f,j}/RT} e^{((1-\beta_j)\Delta E_j)/RT}\left[1 - e^{-\Lambda_j/RT}\right]\prod_i c_i, \quad (1)$$

where $k_j$ is a composition-independent pre-exponential factor, $\Delta G^0_{f,j}$ is the unperturbed free-energy barrier for the reaction step (evaluated at $\Delta E_j = 0$), $\Delta E_j$ is a shift in free energy of reaction associated with a finite driving force (defined in Appendix A and identified below), $\beta_j$ is a reaction symmetry parameter analogous to that used in electrochemical kinetics, $\Lambda_j$ is the total free-energy driving force for the reaction step, and $c_i$ are concentrations of the reacting species in the forward direction whose configurational entropic contribution to the driving force have not been included in $\Delta E_j$. The concentrations $c_i$ represent composition variables expressed in any convenient set of units consistent with the chosen reference state and definition of $k_j$ (e.g., partial pressure, surface concentration or coverage, bulk species concentrations, or mole fractions).

To apply Eq. (1) to an overall reaction, we must first define the elementary steps that constitute the reaction, as well as the free energy of reactants, products, and intermediates involved in those elementary steps. We must then identify the portion of the driving force associated with nonconfigurational shifts in free energy. Finally, we might also wish to hypothesize a specific rate-limiting step, which constitutes the bottleneck to the reaction. In what follows, we apply Eq. (1) to the analysis of $O_2$ reduction on a perovskite mixed conductor, where two asymptotic limits of electronic structure are considered: (a) the material has metallic band structure and thus electrons enter as an energy shift through the Fermi level, and (b) the material is semiconducting, and thus electron holes can enter explicitly through mass action.

### 2.2. Kinetic considerations

Referring to Fig. 1, we must first subdivide the $O_2$-exchange reaction into specific elementary steps, identifying appropriate surface intermediates. Steps commonly considered in the catalysis and ionics literature include $O_2$ adsorption, $O_2$ dissociation, changes in oxidation state of diatomic or monatomic oxygen species, and incorporation of adsorbed O into the bulk. We first try to narrow this list by considering what is known about oxide catalysts. The assumptions stated below are by no means assertions, but rather hypotheses based on limited independent information.

First, we must make some assumptions about the defect structure of the surface. In analogy to bare metals in high vacuum (such as Pt), many workers (including us) have postulated mechanisms in which $O_2^{q-}$ or $O^{q-}$ (of various valances $q$) adsorb as dilute species on the oxide surface [10,20–25]. Although in some cases mass action effects of free surface sites (i.e., Langmuir adsorption) are considered, this is often done with an implicit assumption of low surface coverage. This approach generally defies the conventional wisdom of the oxide catalysis literature, which usually considers the surface to be fully oxidized except for specific coordinatively unsaturated sites, often attributed to surface point defects, step edges, or other surface defects [26–35]. To the best of our knowledge, there is no published evidence that individual oxygen atoms are stable on a fully oxidized surface without bonding to a metal atom. Given these considerations, we assume that adsorption of $O_2$ requires a vacant surface site (analogous to a bulk oxygen vacancy) and that dissociation requires a second vacant surface site to interact with the adsorbed diatomic.

Second, we must consider the valance of monatomic oxygen on the surface. Although workers often consider this an independent variable subject to oxidation or reduction ($O \leftrightarrow O^- \leftrightarrow O^{2-}$) [10,20,21,36], there is currently little independent evidence to support this assumption. For example, XPS and other measurements suggest that dissociatively adsorbed oxygen on Pt adopts a fixed oxidation state (approximately $O^-$), by virtue of its bonding configuration to Pt [37]. This species is the same whether one adsorbs oxygen from the gas or pumps it onto the surface from an electrolyte, such as yttria-stabilized zirconia (YSZ). Likewise, recent density functional calculations suggest that oxide ions at the ceria surface share nearly the same oxidation state as in the bulk [38]. Another way to phrase these observations is that any charge-transfer steps involving monatomic oxygen are fast, and thus only one species is relevant as a reactive intermediate. We assume that the same is true for an oxide mixed conductor—oxide ions at the surface have a fixed oxidation state determined by their bonding configuration. For the moment, we leave the value of this oxidation state as an unknown, returning to this question for specific materials.

Third, we must also consider the identity of adsorbed diatomic intermediates, such as physisorbed $O_2$, superoxide, and peroxide ($O_2 \leftrightarrow O_2^- \leftrightarrow O_2^{2-}$). These species have all been observed on oxide catalysts under certain circumstances of bonding and thus are legitimate possibilities. However, we limit our discussion to cases where the reaction is limited by a specific rate-determining step. In this scenario, we might combine steps before and after the rate-determining step, leaving only one stable intermediate defined explicitly. This does not mean that multiple oxidation states do not occur, but rather that only one of these species is of identifiable kinetic significance. The question then becomes the identity and charge of this critical intermediate, which we also leave as unknown for the moment.

Finally, we also assume that in a material with metallic band structure, considering the mass action of specific electronic point defects (electrons and holes) is not meaningful. In this case, the mechanistic role of electrons is expected to enter

through charge compensation and shifts in electron-free energy. Fleig [21] previously treated electrons in metals as having fixed entropy and internal energy. We believe that these electrons will have fixed entropy but variable internal energy due to changes in Fermi level with respect to core states [9].

With the assumptions outlined above, and adopting Kröger–Vink notation [39] for the charge of oxygen species relative to bulk lattice oxygen, we are left with the following 3-step kinetic description of the $O_2$ reduction reaction:

$$\text{adsorption:}\quad \mathrm{O_2} + \mathrm{V}_{\mathrm{O}_s}^{q_s\cdot} + q_{\mathrm{ads}}e^- \rightleftarrows (\mathrm{O_2})_{\mathrm{O}_s}^{q_{\mathrm{O_2}}\cdot}, \tag{2a}$$

$$\text{dissociation:}\quad (\mathrm{O_2})_{\mathrm{O}_s}^{q_{\mathrm{O_2}}\cdot} + \mathrm{V}_{\mathrm{O}_s}^{q_s\cdot} + q_{\mathrm{diss}}e^- \rightleftarrows 2\mathrm{O}_{\mathrm{O}_s}^{q_{\mathrm{O}}\cdot}, \tag{2b}$$

$$\text{incorporation:}\quad \mathrm{O}_{\mathrm{O}_s}^{q_{\mathrm{O}}\cdot} + \mathrm{V}_{\mathrm{O}_b}^{\cdot\cdot} + q_{\mathrm{incorp}}e^- \rightleftarrows \mathrm{O}_{\mathrm{O}_b}^{X} + \mathrm{V}_{\mathrm{O}_s}^{q_s\cdot}, \tag{2c}$$

and

$$\text{overall reaction:}\quad \mathrm{O_2} + 2\mathrm{V}_{\mathrm{O}_b}^{\cdot\cdot} + 4e^- \rightleftarrows 2\mathrm{O}_{\mathrm{O}_b}^{X}, \tag{2d}$$

where the primary symbols $O_2$, V, and O refer to diatomic oxygen, oxygen vacancies, and oxygen atoms, respectively. The subscripts $O_s$ and $O_b$ refer to species location at a surface or bulk oxygen site, respectively. The superscripts indicate species charge relative to a normal lattice oxygen ion (see Appendix B for further explanation of Kröger–Vink notation), and $q_{\mathrm{ads}}q_{\mathrm{diss}}$, and $q_{\mathrm{incorp}}$ are the charge transferred in each of the three steps. Imposing charge balance, we require

$$q_s = q_{\mathrm{O}} + \frac{q_{\mathrm{ads}} + q_{\mathrm{diss}}}{2}, \tag{3a}$$

$$q_{\mathrm{O_2}} = q_{\mathrm{O}} - \frac{(q_{\mathrm{ads}} - q_{\mathrm{diss}})}{2}, \tag{3b}$$

$$q_{\mathrm{ads}} + q_{\mathrm{diss}} + 2q_{\mathrm{incorp}} = 4. \tag{3c}$$

Due to electroneutrality and site conservation, these species cannot change concentration independently. Even at the surface, where charges are separated across an interface, Gauss's law requires that the entire interface (including associated double layers) be neutral. Thus for purposes of defining thermodynamic relationships, it is useful to adopt a *neutral building-unit* convention. Let us define

$$s = \left\{V_{\mathrm{O}_s}^{q_s\cdot} + (q_s - q_{\mathrm{O}})e^- - \mathrm{O}_{\mathrm{O}_s}^{q_{\mathrm{O}}\cdot}\right\}, \tag{4a}$$

$$s\mathrm{O_2} = \left\{(\mathrm{O_2})_{\mathrm{O}_s}^{q_{\mathrm{O_2}}\cdot} + (q_{\mathrm{O_2}} - q_{\mathrm{O}})e^- - \mathrm{O}_{\mathrm{O}_s}^{q_{\mathrm{O}}\cdot}\right\}, \tag{4b}$$

and

$$\nu = \left\{V_{\mathrm{O}}^{\cdot\cdot} + 2e^- - O_{\mathrm{O}}^{X}\right\}. \tag{4c}$$

Fig. 3 illustrates the system configurations associated with these three neutral building units.

A building unit convention is a convenient way of incorporating lattice site conservation into thermodynamic and transport laws [39]. In this case, we have extended this building unit convention to also include charge compensation. As explained by Newman, this approach avoids the problem of defining activities of charged species [15]. The way in which the species in Eq. (4) have been defined (Fig. 3), they are neutral entities and thus have well-defined chemical potentials independent of electrical state. If this were an electrochemical reaction (involving current across an interface between two phases), then the chemical potential of the surface building units would need to be expressed in terms of a difference in electrical state between the two phases. However, for a chemical interface (no current), this difference is determined by surface coverage (dipole) and thus is experimentally indistinguishable from other shifts in adsorption enthalpy.

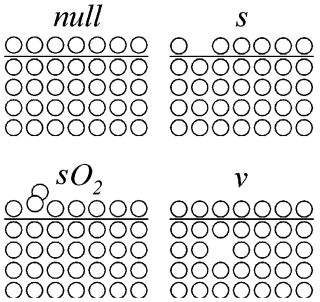


Fig. 3. Configurations corresponding the neutral building units defined in Eq. (4). Absence of a formal charge assignment reflects the fact that the bulk and interface remain electrically neutral as a whole (not that individual species are uncharged). Energetic effects of charge separation are included in the building unit free energies (see text).

It should be emphasized that the adoption of a neutral building unit convention in Eq. (4) does not imply that the electrochemical potential of bulk or surface species are independent of local Galvani potential. For example, recent models by Fleig [21] and Mebane [22] defined electrochemical potential of surface species in terms of a surface potential and examined how shifts in surface potential enter as an energy-shift component of the driving force. The approach here does not conflict with,or preclude such models. Here we have simply bundled these contributions together into the definition of the building unit. As with moderately dilute or concentrated solutions [15], this approach avoids defining more thermodynamic variables than are independently measurable. As we will discuss further below, the role of individual species entropy (or energy) may be identified explicitly later as desired, depending on one's particular microscopic model of the surface (including metallic vs semiconducting materials and $n$-type vs $p$-type materials).

With this approach, only molecular, ionic, and adsorbate mass action remain defined explicitly in the following reaction steps:

$$\text{adsorption:}\quad \mathrm{O_2} + s \rightleftarrows s\mathrm{O_2}, \tag{5a}$$

$$\text{dissociation:}\quad s\mathrm{O_2} + s \rightleftarrows \text{null}, \tag{5b}$$

$$\text{incorporation:}\quad \nu \rightleftarrows s, \tag{5c}$$

and

$$\text{overall reaction:}\quad \mathrm{O_2} + 2\nu \rightleftarrows \text{null}. \tag{5d}$$

Applying Eq. (1), our kinetic rate laws for the three reactions become

$$r_{\mathrm{ads}} = k_{\mathrm{ads}}e^{-\Delta G^0_{f,\mathrm{ads}}/RT} P_{\mathrm{O_2}} \Gamma_s e^{((1-\beta_{\mathrm{ads}})\Delta E_{\mathrm{ads}})/RT} \times \left[1 - e^{-\Lambda_{\mathrm{ads}}/RT}\right], \tag{6a}$$

$$r_{\mathrm{diss}} = k_{\mathrm{diss}}e^{-\Delta G^0_{f,\mathrm{diss}}/RT} \Gamma_s \Gamma_{s\mathrm{O_2}} e^{((1-\beta_{\mathrm{diss}})\Delta E_{\mathrm{diss}})/RT} \times \left[1 - e^{-\Lambda_{\mathrm{diss}}/RT}\right], \tag{6b}$$

and

$$r_{\text{incorp}} = k_{\text{incorp}} e^{-\Delta G^0_{f,\text{incorp}}/RT} x_v e^{((1-\beta_{\text{incorp}})\Delta E_{\text{incorp}})/RT} \times \left[1 - e^{-\Lambda_{\text{incorp}}/RT}\right], \quad (6c)$$

where $P_{O_2}$ is the partial pressure of oxygen in the gas relative to atmospheric pressure, $\Gamma_i$ is the fraction of active surface sites occupied by species $i$, $x_v$ is the fraction of bulk oxygen lattice sites occupied by a vacancy, and $\Delta E_j$ is the energy-shift component of the thermodynamic driving force for the $j$th reaction, as derived below. Under quasi-steady conditions, the rate of the three reactions are related to the overall reaction (and each other) by

$$r = r_{\text{ads}} = r_{\text{diss}} = \frac{r_{\text{incorp}}}{2}. \quad (7)$$

### 2.3. Thermodynamic considerations for systems with metallic band structure

To proceed, we now introduce a set of thermodynamic relationships between the various species concentrations and chemical potentials of the building units. We reemphasize that we must consider the chemical potential of the entire building unit, which includes multiple atomic and electronic species and any energetic interactions among them. Although the charge separation at the interface can be expressed in terms of a difference in inner potential between surface and bulk [21,22], this potential difference is a function of composition, and thus it appears here as an energy contribution to the chemical potential of the neutral building unit with no loss of generality.

In most of the materials that we consider, the bulk vacancy concentration remains small, and thus it is reasonable to assume that the configurational entropy of lattice oxygen ($O_O^X$) remains constant, obeying the solvent approximation (up to ∼10% error in some cases). Although in general we expect the surface chemistry to be different than the bulk, we recognize that the material is an oxide and as such is highly oxidized even at the surface. Thus, we likewise assume that the fractions of free surface vacancies ($\Gamma_s$) and adsorbed diatomic intermediates ($\Gamma_{sO_2}$) are relatively small compared with the concentrations of oxidized sites, which remain relatively close to saturation and thus also obey the solvent approximation.

For metallic mixed conductors, such as $La_{1-x}Sr_xCoO_{3-\delta}$, Lankhorst has developed a model for the chemical potential of bulk neutral vacancy building units ($v$), as defined in Eq. (4c). The primary assumption of Lankhorst's model is that electron entropy remains roughly constant, whereas electron energy depends linearly on electron occupation within a metallic or broadly manifolded band of states. Thus the configurational entropy of the building unit is dominated by vacancies, whereas the internal energy is dominated by shifts in Fermi energy on changes in oxidation state (related to vacancy concentration through electroneutrality). With the addition of the solvent approximation, Lankhorst's model predicts

$$\mu_v = \mu_v^0(x) + RT\ln(x_v) + 2E_F(x_v), \quad (8)$$

where $x$ is the number of acceptor dopants per 3 oxygen sites (e.g., mole fraction of Sr on La/Sr sites in $La_{1-x}Sr_xCoO_{3-\delta}$),

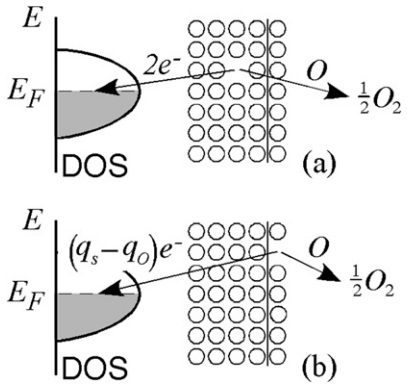


Fig. 4. Charge separation created by an oxygen atom being removed from (a) the bulk ($v$) or (b) the surface ($s$) as $\frac{1}{2}O_2$. In metallic mixed conductors, liberated electrons join band states at the Fermi level, which is a function of composition [9].

$\mu_v^0(x) = -\frac{1}{2}(E_{\text{ox}} - TS_{\text{ox}} + 4x/g_0)$ is the standard free energy of a neutral vacancy building unit, and

$$E_F(x_v) = 6x_v/g_0 \quad (9)$$

is the Fermi energy measured relative to its value at full oxygen stoichiometry, where $g_0$ is the density of states at the Fermi level in the bulk, assumed to be constant [9].

The second term on the right side of Eq. (8) represents the normal shift in bulk vacancy chemical potential with vacancy configurational entropy. The last term in Eq. (8) reflects the positive shift in electron energy relative to core states as the material is reduced. This latter process is depicted qualitatively in Fig. 4a. When a vacancy is created by pulling an oxygen atom out of the bulk, the average oxidation state of the transition metal must decrease, resulting in an increase in electron energy. This model has been found to agree well with gravimetric and coulometric nonstoichiometry measurements in $La_{1-x}Sr_xCoO_{3-\delta}$, over a wide range of $x$, $T$, and $P_{O_2}$ [40].

To predict $\mu_s$, we must similarly consider how shifts in Fermi energy might affect the stability of surface vacancies. To begin, let us imagine the surface as a net electrically neutral interface, with a surface dipole related to the charge separation between surface species and their mirror charges in the bulk. This charge separation is similar conceptually to the internal charge separation between oxygen vacancies and free electrons in the bulk. Thus we might expect a relationship similar to that in Eq. (8) to prevail.

How charge separation at the surface and other adsorbate interactions influence the energy of adsorption is a subject of great debate and uncertainty [41]. For dilute semiconductors, workers often explicitly describe the effect of charge separation on the energy of adsorption [42]. Some workers have applied similar ideas to dissociative adsorption on mixed conductors, defining a composition-dependent surface potential, $\chi$, as the difference in Galvani potential between surface and bulk [21,22]. However, this approach assumes that all other energetic contributions remain constant as a function of surface coverage. Experimental and theoretical studies of charge-compensated adsorption on metal and oxide catalysts have led to little consensus as to whether adsorption enthalpy actually changes with

coverage in this manner [41]. Workers have generally shown that reconstruction or other adjustments to the local electronic structure can be as significant as surface dipole effects, leading to positive, negative, or zero shifts in enthalpy with coverage [43–45]. Because surface dipole effects are experimentally inseparable from these other energetic interactions, the introduction of $\chi$ in this context is of limited utility. Studies of $O_2$, CO, and NO adsorption on single-crystal Pt, Ni, and Rh show that variations in adsorption enthalpy with coverage in the range of interest here are generally smaller than differences among different crystal faces [43]. Thus, in the absence of better information, we assume that the energy of adsorption is independent of surface vacancy concentration.

But because the material is a good electronic conductor, we expect the Fermi level seen by species on the surface to be the same as that in the bulk [15] (assuming that electrons remain in equilibrium). Although changes in surface species concentrations will contribute negligibly to shifts in the bulk Fermi energy, the Fermi energy remains dependent on bulk composition. Thus, even without surface dipole effects, we expect an energy contribution due to electronic equilibrium with the bulk,

$$\mu_s = \mu_s^0 + RT\ln(\Gamma_s) + (q_s - q_O)E_F(x_v), \tag{10}$$

where $q_s - q_O$ is the change in surface charge created when a lattice oxygen at the surface is replaced by a surface vacancy (Fig. 4b). For example, if oxygen ions on the surface have the same partial charge as they do formally in the bulk ($O^{2-}$), then $q_s - q_O = 2$, and thus the energetic dependence of the surface vacancy chemical potential on $x_v$ would be the same as for bulk vacancies. Likewise, if the charge on surface atoms were zero, then $q_s - q_O = 0$, and the chemical potential of unoccupied sites would depend only on their configurational entropy. How $\mu_s^0$ depends on bulk acceptor doping ($x$) is unknown. For example, in $La_{1-x}Sr_xCoO_{3-\delta}$, any preference for La or Sr at the surface might tend to alter the dependency of $\mu_s^0$ on $x$ relative to $\mu_v^0(x)$.

Extending the same arguments to adsorbed molecular oxygen, we also have

$$\mu_{sO_2} = \mu_{sO_2}^0 + RT\ln(\Gamma_{sO_2}) + (q_{O_2} - q_O)E_F(x_v). \tag{11}$$

### 2.4. Identification of the entropic and energetic components of the driving force

From here, the procedure is straightforward. Substitution of Eqs. (8)–(11) into the equilibria of Eq. (5) yields

$$0 = RT\ln\left(\frac{P_{O_2}\Gamma_s}{\Gamma_{sO_2}}\right) - \left(\mu_{sO_2}^0 - \mu_{O_2}^0 - \mu_s^0\right) + q_{ads}E_F, \tag{12a}$$

$$0 = RT\ln(\Gamma_{sO_2}\Gamma_s) - \left(-\mu_{sO_2}^0 - \mu_s^0\right) + q_{diss}E_F, \tag{12b}$$

$$0 = RT\ln\left(\frac{x_v}{\Gamma_s}\right) - \left(\mu_s^0 - \mu_v^0(x)\right) + q_{incorp}E_F, \tag{12c}$$

and overall reaction:

$$0 = RT\ln\left(P_{O_2}x_v^2\right) - \left(-\mu_{O_2}^0 - 2\mu_v^0(x)\right) + 4E_F. \tag{12d}$$

From Eq. (12), the entropic and nonideal energetic components of the free-energy driving forces for each reaction can be readily identified and described in the form

$$\Lambda_j = RT\ln Q_j - \Delta G_j^0 + \Delta E_j, \tag{13}$$

with values of $Q_j$, $\Delta G_j^0$, and $\Delta E_j$ given in Table 1 for the three steps in Eq. (5). Substitution of Eq. (13) into Eq. (6) for each of the three reactions yields a complete set of kinetic rate expressions that can be solved for a given overall driving force (in terms of $P_{O_2}$ and $x_v$), as well as kinetic and thermodynamic parameters.

Table 1
Components of thermodynamic driving force for adsorption, dissociation, and incorporation of oxygen into a mixed conducting oxide (see Eqs. (5), (6), and (13))

| Step ($j$) | $Q_j$ | $\Delta E_j$ | $\Delta G_j^0$ |
|---|---|---|---|
| Adsorption | $\frac{P_{O_2}\Gamma_s}{\Gamma_{sO_2}}$ | $q_{ads}E_F$ | $\mu_{sO_2}^0 - \mu_{O_2}^0 - \mu_s^0$ |
| Dissociation | $\Gamma_s\Gamma_{sO_2}$ | $q_{diss}E_F$ | $-\mu_{sO_2}^0 - \mu_s^0$ |
| Incorporation | $\frac{x_v}{\Gamma_s}$ | $q_{incorp}E_F$ | $\mu_s^0 - \mu_v^0$ |
| Total reaction | $P_{O_2}x_v^2$ | $4E_F$ | $-\mu_{O_2}^0 - 2\mu_v^0$ |

The last line in Table 1 reveals that the overall driving force for the reaction is a displacement in the bulk vacancy concentration for equilibrium with the gas,

$$\begin{aligned}\Lambda &= RT\ln\left(P_{O_2}^{gas}x_v^2\right) - \Delta G_{rxn}^0(x) + 4E_F \\ &= RT\ln\left(\frac{P_{O_2}^{gas}}{f_{O_2}^{solid}}\right),\end{aligned} \tag{14}$$

where for convenience we have reexpressed the bulk vacancy mole fraction $x_v$ in terms of the oxygen fugacity in the solid, $f_{O_2}^{solid}$, defined as the $P_{O_2}$ that would be in equilibrium with the solid at composition $x_v$. The variables $f_{O_2}^{solid}$ and $x_v$ are interrelated by Eq. (14) when $f_{O_2}^{solid} = P_{O_2}^{gas}$:

$$f_{O_2}^{solid} = x_v^{-2}e^{(\Delta G_{rxn}^0(x) - 24x_v/g_0)/RT} \tag{15a}$$

and

$$x_v = \frac{g_0RT}{12}W\left(\frac{12}{g_0RT}e^{(\Delta G_{rxn}^0(x))/2RT}\left(f_{O_2}^{solid}\right)^{-1/2}\right), \tag{15b}$$

where $W(z)$ is Lambert's function, defined such that $z = W(z)e^{W(z)}$. These variables can then be related to the Fermi energy via Eq. (9). Equation (15), which is an expression of equilibrium within the solid phase, also demonstrates that the kinetics obey thermodynamics in the limit of equilibrium.

Assuming that the driving force $\Lambda$ is known, the net rate of the reaction $r$ can be determined by simultaneous application of Eqs. (13)–(15), with $E_F(x_v)$ given by Eq. (9). In general, this is a transcendental problem requiring simultaneous numerical calculation of the reactive intermediate concentrations.

### 2.5. Introduction of a rate-determining step

An enormous simplification of the kinetics in Eqs. (13)–(15) is possible if one the three steps ($m$) in Eq. (5) is rate-determining, whereas the others ($j \neq m$) are quasi-equilibrated.

Table 2
Stoichiometric ratio and rate prefix associated with each of various rate-limiting steps (see Eqs. (16) and (17))

| Limiting step | $\lambda_m$ | $RT\ln\Re_{0,m}$ |
|---|---|---|
| Adsorption (Eq. (5a)) | 1 | $RT\ln\frac{k_{\rm ads}P_{\rm O_2}}{\sqrt{f_{\rm O_2}^{\rm solid}}}-\Delta G^0_{f,\rm ads}+\frac{\Delta G^0_{\rm ads}+\Delta G^0_{\rm diss}}{2}+\frac{q_{\rm ads}(1-2\beta_{\rm ads})-q_{\rm diss}}{2}E_F(f_{\rm O_2}^{\rm solid})$ |
| Dissociation (Eq. (5b)) | 1 | $RT\ln\left(\frac{k_{\rm diss}P_{\rm O_2}^{\rm gas}}{f_{\rm O_2}^{\rm solid}}\right)-\Delta G^0_{f,\rm dis}+\Delta G^0_{\rm dis}-\beta_{\rm dis}q_{\rm dis}E_F(f_{\rm O_2}^{\rm solid})$ |
| Incorporation (Eq. (5c)) | 2 | $RT\ln\left(\frac{k_{\rm incorp}}{2\sqrt{f_{\rm O_2}^{\rm solid}}}\right)-\Delta G^0_{f,\rm incorp}+\frac{\Delta G^0_{\rm rxn}}{2}-((1-\beta_{\rm incorp})q_{\rm incorp}-2)E_F(f_{\rm O_2}^{\rm solid})$ |

Table 3
Predicted dependency of $\Re_0$ on $P_{\rm O_2}$ and $T$ for each of the limiting steps in Table 2 (see Eqs. (25)–(29))

| Limiting step | $n=\left.\frac{\partial\ln\Re_0}{\partial\ln P_{\rm O_2}^{\rm eqb}}\right\vert_T$ | $E_A^{\rm eff}=-\left.\frac{\partial\ln\Re_0}{\partial(1/RT)}\right\vert_{P_{\rm O_2}}$ |
|---|---|---|
| Adsorption (Eq. (5a)) | $\frac{1}{2}+\frac{q_{\rm diss}-(1-2\beta_{\rm ads})q_{\rm ads}}{8}(1+2\gamma)$ | $\Delta H^0_{f,\rm ads}-\frac{\Delta H^0_{\rm ads}+\Delta H^0_{\rm diss}}{2}+\frac{q_{\rm diss}-q_{\rm ads}(1-\beta_{\rm ads})}{2}\frac{\partial(E_F/RT)}{\partial(1/RT)}$ |
| Dissociation (Eq. (5b)) | $\frac{\beta_{\rm diss}q_{\rm diss}}{4}(1+2\gamma)$ | $\Delta H^0_{f,\rm diss}-\Delta H^0_{\rm diss}+\beta_{\rm diss}q_{\rm diss}\frac{\partial(E_F/RT)}{\partial(1/RT)}$ |
| Incorporation (Eq. (5c)) | $\gamma-\frac{(1-\beta_{\rm incorp})q_{\rm incorp}}{4}(1+2\gamma)$ | $\Delta H^0_{f,\rm incorp}-\frac{\Delta H^0_{\rm rxn}}{2}+(2-(1-\beta_{\rm incorp})q_{\rm incorp})\frac{\partial(E_F/RT)}{\partial(1/RT)}$ |

In this limit, the driving force for the rate-limiting reaction step ($\Lambda_m$) becomes proportional to the total driving force $\Lambda$, whereas the driving forces for the other two reactions ($\Lambda_{j\neq m}$) approach zero [46]:

$$\Lambda_m=\frac{\Lambda}{\lambda_m}=\frac{RT}{\lambda_m}\ln\left(\frac{P_{\rm O_2}^{\rm gas}}{f_{\rm O_2}^{\rm solid}}\right)\quad\text{and}\quad\Lambda_{j\neq m}=0, \tag{16}$$

where $\lambda_m=r_m/r$ is the stoichiometric ratio between $r_m$ and $r$ under quasi-steady conditions.

Substitution of Eq. (16) into Eq. (13) allows the concentrations of the surface intermediates ($\Gamma_s$, $\Gamma_{s\rm O_2}$) to be reexpressed in terms of $P_{\rm O_2}^{\rm gas}$ and $f_{\rm O_2}^{\rm solid}$. The rate is then determined by the rate expression for the $m$th step according to Eqs. (6) and (16). The result can be written in the form

$$r=\Re_{0,m}\left[1-e^{-\Lambda/(\lambda_m RT)}\right], \tag{17}$$

where $\lambda_m$ and $\Re_{0,m}$ are given in Table 2 for each of the three steps as rate-limiting. In these expressions, the variables $f_{\rm O_2}^{\rm solid}$ and $x_v$ are interchangeable according to Eq. (15).

### 2.6. Extension of the analysis to P-type semiconductors

We now extend the theory in Sections 2.1–2.5 for the case of a mixed conductor with more localized band structure. Unlike in a metal, the energies of electrons and holes in a semiconductor are determined by the energies of the (fixed) band edges [15], and thus (to first approximation) are independent of electron occupation. Meanwhile, the configurational entropies of electrons and holes are not fixed (as in a metal), but are expected to vary according to mass action. With these simplifications, we expect rate expressions derived by previous workers (under the assumption of point defect theory [10,20–22]) to already be consistent with thermodynamics. However, here we depart from previous models in two ways. First, unlike many models that assume low surface coverage, we apply the assumptions of Section 2.2, in which adsorbates must compete for a small number of surface oxygen vacancies. Second, instead of incorporating electron or hole mass action in the kinetics (from the beginning), we show, using our formalism, that $n$-type, $p$-type, or $p$–$n$ transitional materials can all be treated using a single rate expression by incorporating electron and hole configurational entropy into the thermodynamics. Electron or hole mass action emerges naturally when shifts in Fermi energy are accounted for in terms of electron and hole concentrations.

With this approach, Eqs. (5)–(14) and Tables 1–3 remain valid for a semiconductor as well as for a metal, with the exception of Eq. (9). The distinction arises in treating the relationship of Fermi energy to composition and temperature, $E_F(f_{\rm O_2}^{\rm solid},T)$. Instead of Lankhorst's model for a metallic mixed conductor, we must instead apply a model appropriate to a semiconductor. Following Newman's treatment of semiconductor electrodes [15], the Fermi energy can be written in terms of electron or hole entropies as

$$E_F=-RT\ln\left(\frac{c_h}{N_{\rm VB}}\right)=E_{\rm gap}+RT\ln\left(\frac{c_e}{N_{\rm CB}}\right), \tag{18}$$

where $E_F$ is defined relative to the valance band edge, $c_e$ and $c_h$ are the electron and hole concentrations, $E_{\rm gap}$ is the band gap, and $N_{\rm VB}$ and $N_{\rm CB}$ are the effective densities of states of the valance and conduction bands, respectively. Equation (18) can be rearranged to reveal electron–hole equilibrium,

$$\left(\frac{c_e}{N_{\rm CB}}\right)\left(\frac{c_h}{N_{\rm VB}}\right)=x_e x_h=e^{-E_{\rm gap}/RT}=K_{\rm np}, \tag{19}$$

where $K_{\rm np}$ is an equilibrium constant for electron and hole creation (defined in terms of fractional band occupancies, $x_e$ and $x_h$). Concentrations of electrons, holes, and oxygen vacancies are further constrained by electroneutrality [47]

$$2c_0x_v+N_{\rm VB}x_h-N_{\rm CB}x_e-\frac{c_0x}{3}=0, \tag{20}$$

where $x$ is the number of acceptor dopants per 3 oxygen sites. Simultaneous application of Eqs. (18)–(20) and Eq. (14) (with $\Lambda = 0$) allow $x_v$, $x_h$, and $x_e$ to be expressed in terms of $f_{O_2}^{\text{solid}}$, thus completing the connection between $E_F$ and $f_{O_2}^{\text{solid}}$. The rate expressions for the three rate-limiting steps discussed in Section 2.5 are then given in Table 2.

### 2.7. Connection to mass action for n-type and p-type materials

Note that in Eq. (14), electron or hole populations enter the driving force through $E_F$, rather than as explicit mass action effects. Because we have assumed point defect theory, we expect these views to be equivalent. To see this, we can examine the individual rate laws with the electron or hole concentrations identified explicitly. As an example, the dissociation step [Eq. (6b)] can be rearranged as

$$r_{\text{diss}} = k_{\text{diss}} e^{-\Delta G^0_{f,\text{diss}}/RT} e^{(1-\beta_{\text{diss}})q_{\text{diss}}E_{\text{gap}}/RT} \Gamma_s \Gamma_{sO_2} x_e^{(1-\beta_{\text{diss}})q_{\text{diss}}} \times \left[1 - e^{-\Lambda_{\text{diss}}/RT}\right]. \tag{21a}$$

If $\beta_{\text{diss}} = 0$ (barrier height remains fixed for the reverse reaction), this can be further rearranged into a simple mass action rate expression of order $x_e^{q_{\text{diss}}}$ in the forward direction,

$$r_{\text{diss}} = k_{\text{diss}} e^{(-\Delta G^0_{f,\text{diss}} + q_{\text{diss}}E_{\text{gap}})/RT} \Gamma_s \Gamma_{sO_2} x_e^{q_{\text{diss}}} - k_{\text{diss}} e^{-\Delta G^0_{b,\text{diss}}/RT}, \tag{21b}$$

where $q_{\text{diss}}$ is the number of electrons transferred (including upstream equilibrated steps). The forward Arrhenius factor includes the band gap, because we arbitrarily defined the valance band energy as zero.

Likewise, for a purely $p$-type semiconductor, we expect the hole concentration to enter through the *reverse* reaction rate. This corresponds to the case where $\beta = 1$ (the barrier height remains fixed for the forward reaction). This can be seen by rearranging Eq. (6b) once again,

$$r_{\text{diss}} = k_{\text{diss}} e^{-\Delta G^0_{f,\text{diss}}/RT} \Gamma_s \Gamma_{sO_2} - k_{\text{diss}} e^{-\Delta G^0_{b,\text{diss}}/RT} x_h^{q_{\text{diss}}}, \tag{21c}$$

where the reverse reaction is or order $x_h^{q_{\text{diss}}}$ (including downstream equilibrated steps).

If an energy barrier to charge transfer exists, then the value of $\beta$ is expected to deviate from 0 or 1 even in a pure $n$-type or $p$-type material. Likewise, if no energy barrier exists, but the material is near a $p$–$n$ transition, then $\beta$ is also expected to be between 0 and 1, depending on the relative importance of electrons or holes in the charge-transfer process. Finally, for systems with a small band gap, or materials undergoing a metal–insulator transition, it becomes less meaningful to treat electrons and holes explicitly, and thus the case of $0 < \beta < 1$ could represent a mix of mass action and energetic effects. These examples illustrate the fundamental inseparability of mass action and energetic effects in systems with complex electronic structure. In the absence of detailed independent information about these factors, the interpretation of a measured noninteger $\beta$ is not likely to be unique.

## 3. Comparison of model predictions to published equilibrium exchange rates for metallic $La_{1-x}Sr_xCoO_{3-\delta}$ and $p$-type $La_{1-x}Sr_xFeO_{3-\delta}$

### 3.1. Challenges to comparing theory with experimental data

Although many workers have measured $O_2$-exchange kinetics on perovskite mixed conductors, a direct comparison of these measurements to Eq. (17) and Table 2 is challenging. First, the vast majority of these measurements have been made under equilibrium or near-equilibrium conditions. In this situation, it is not possible to probe the bracketed force–flux relationship in Eq. (17) directly. Instead, workers have generally tried to measure the limiting equilibrium value of $\Re_0$ (exchange rate) over a range of governing parameters such as $T$ and $P_{O_2}$, and then compared these dependencies to models for the mechanism.

Second, the techniques used to measure these equilibrium-exchange rates typically require a significant level of modeling and interpretation. For example, one popular class of methods involves equilibrating a sample at a chosen $T$ and initial $P^0_{O_2}$, and then stepping the $P_{O_2}$ suddenly by some small amount to a new value, $P^1_{O_2}$. The average vacancy concentration in the sample is then monitored as it approaches equilibrium, using an appropriate secondary indicator, such as electrical conductivity, lattice volume, or mass [2–6]. The data are then fit to a linear model for the kinetics and diffusion. The exchange rate can then be calculated from the surface rate coefficient by linearization of Eq. (17),

$$\Re_0 = \lambda RT \left(\frac{\partial r}{\partial \Lambda}\right)_T, \tag{22}$$

where $(\partial r/\partial \Lambda)_T$ is the surface rate coefficient, written here in terms of a chemical potential driving force.

In interpreting these measurements, workers usually make the assumption of linearity. But the $P_{O_2}$ step sizes used are seldom small enough to rigorously qualify as linear, and thus misattribution of nonexponential kinetic relaxation to diffusion is likely. In measurements of expansion relaxation of $La_{1-x}Sr_xCoO_{3-\delta}$, we have also found evidence of strong hysteresis in the surface exchange coefficient, further complicating interpretation (X.Y. Chen and S.B. Adler, unpublished data). In addition, to obtain $\Re_0$ from Eq. (17), we must specify $\lambda$, which is usually not known a priori. We must assume a rate-determining step involving diatomic oxygen for $\lambda = 1$. Finally, workers often do not calculate $\Re_0$, but rather report $(\partial r/\partial \Lambda)_T$ in the form of a linearized rate coefficient specific to a particular species (e.g., $k^\delta$ [10], $K_{\text{ex}}$ [48], or $K_{\text{tr}}$ [49]). To use Eq. (22), we must know the thermodynamic properties of the material to convert these other coefficients to $RT(\partial r/\partial \Lambda)_T$ (in mol of $O_2/cm^2/s$). As an example, if we define oxygen flux to the surface as $r = -\frac{1}{2}K_{\text{tr}}([O_O^X]^{\text{eqb}} - [O_O^X])$ [49], then $RT(\partial r/\partial \Lambda)_T$ is calculated as

$$RT\left(\frac{\partial r}{\partial \Lambda}\right)_T = -\frac{\partial r}{\partial \ln(f_{O_2}^{\text{solid}})} = -x_v \frac{\partial r}{\partial x_v}\gamma = x_v c_0 \frac{\partial r}{\partial [O_O^X]}\gamma = -x_v c_0 \frac{K_{\text{tr}}}{2}\gamma, \tag{23}$$

where $c_0$ is the oxygen site concentration in the lattice and

$$\gamma = \left(\frac{\partial \ln x_v}{\partial \ln f_{O_2}^{solid}}\right)_T \tag{24}$$

is a thermodynamic factor relating vacancy concentration and $P_{O_2}$.

As an alternative to the transient driving force experiments discussed above, workers have also tried to measure $\Re_0$ "directly" using isotope tracer techniques. In this experiment, the sample is first equilibrated at $T$ and $P_{O_2}$, and then the $^{16}O_2$ in the sample chamber is replaced by $^{18}O_2$. Some time later the sample is quenched, and the isotope profile is fit to determine the tracer diffusion coefficient $D^*$ and $k^* = 2\Re_0/c_0$, where $k^*$ is the surface isotope-exchange coefficient [8]. Although knowledge of λ is not required in this experiment, it must be assumed that there are no other parallel mechanisms by which the isotope may exchange with the solid [10]. For example, imagine that adsorbed $^{18}O_2$ could directly swap one labeled oxygen atom for an unlabeled atom from the solid to form $^{18}O^{16}O$, without ever crossing the full dissociation barrier [11]. If this process has a lower activation energy than dissociative exchange, then it will occur at a faster rate. Workers usually do not consider this possibility, but it is a source of uncertainty if the mechanism turns out to involve an energetic barrier to $O_2$ dissociation.

### 3.2. Predicted dependence of the equilibrium exchange rates on T and $P_{O_2}$

Given the issues outlined above (and the fact that most exchange data are reported on a log–log or Arrhenius plot), one approach to comparing Eq. (17) to exchange data is in terms of the local $T$ and $P_{O_2}$ dependencies of $\Re_0$. This can be accomplished straightforwardly by replacing both $P_{O_2}^{gas}$ and $f_{O_2}^{solid}$ in Eq. (17) with the equilibrium value, $P_{O_2}^{eqb}$, and then taking the derivative with respect to $T$ and $P_{O_2}^{eqb}$. This calculation yields the local $P_{O_2}$ exponent of the exchange rate, $n = (\partial \ln \Re_0/\partial \ln P_{O_2}^{eqb})_T$, and an effective Arrhenius energy, $E_A^{eff} = -(\partial \ln \Re_0/\partial(1/RT))_{P_{O_2}}$. The results for the three limiting steps outlined in Table 2 are given in Table 3, where we have also defined $\Delta H_i = \Delta G_i + T\Delta S_i$.

As part of this calculation, it is necessary to determine the dependencies of $E_F$ on $f_{O_2}$ and $T$. For a metallic mixed conductor, these dependencies are given by

$$\left.\frac{\partial E_F}{\partial \ln f_{O_2}^{solid}}\right|_T = -\frac{RT}{4}(1+2\gamma) \tag{25a}$$

and

$$\frac{\partial(E_F/RT)}{\partial(1/RT)} = \frac{\Delta H_{rxn}^0 + 2RT}{4}(1+2\gamma), \tag{25b}$$

where

$$\gamma = \left.\frac{\partial \ln x_v}{\partial \ln f_{O_2}^{solid}}\right|_T = -\frac{1}{2}\left(1 + W\left(\varepsilon/\sqrt{f_{O_2}^{solid}}\right)\right)^{-1} \tag{26a}$$

and

$$\varepsilon = \frac{12}{g_0 RT} e^{(\Delta G_{rxn}^0(x))/2RT}, \tag{26b}$$

where $\varepsilon$ is a dimensionless group reflecting the relative importance of electron energy versus vacancy configurational entropy. We likewise can calculate the analogous quantities for a $p$-type mixed conductor. Let us assume that electrons contribute negligibly to electroneutrality ($x_e = 0$ in Eq. (20). This allows the internal defect equilibria [Eqs. (14), (19), and (20), with $\Lambda = 0$] to be solved in closed form for $E_F(f_{O_2}^{solid})$. The result is

$$E_F = -RT \ln\left(\frac{-4x_h^{max}\gamma}{(1-2\gamma)}\right), \tag{27}$$

where

$$\gamma = \frac{\partial \ln x_v}{\partial \ln f_{O_2}^{solid}} = -\frac{1}{2}\left(1 + \varepsilon/\sqrt{f_{O_2}^{solid}}\right)^{-1/2} \tag{28a}$$

and

$$\varepsilon = 4\left(x_h^{max}/x_h^{\infty}\right)^2, \tag{28b}$$

and

$$x_h^{max} = \lim_{f_{O_2}^{solid}\to\infty} x_h = \frac{c_0 x}{3N_{vb}}, \tag{28c}$$

$$x_h^{\infty} = \frac{\lim_{f_{O_2}^{solid}\to 0} x_h}{(f_{O_2}^{solid})^{1/4}} = e^{-\Delta G_{rxn}^0/4RT}\sqrt{\frac{x}{6}}, \tag{28d}$$

where here the dimensionless group $\varepsilon$ takes on a slightly different meaning than it did for a metal. For a $p$-type semiconductor, it reflects the relative importance of hole configurational entropy versus vacancy configurational entropy. Taking derivatives with respect to $f_{O_2}^{solid}$ and $1/RT$, we obtain

$$\left.\frac{\partial E_F}{\partial \ln f_{O_2}^{solid}}\right|_T = -\frac{RT}{4}(1+2\gamma) \tag{29a}$$

and

$$\left.\frac{\partial(E_F/RT)}{\partial(1/RT)}\right|_{f_{O_2}^{solid}} = \frac{1}{4}\Delta H_{rxn}^0(1+2\gamma). \tag{29b}$$

Comparing Eqs. (25) and (29) shows that the effect of bulk vacancy defect thermodynamics on the exchange kinetics is nearly the same for metallic and semiconducting materials and can be summarized by a single function: $\gamma(T, P_{O_2})$. In other words, given the same kinetic assumptions, a metallic and semiconducting material will still differ substantially due to fundamental differences in thermodynamic behavior. This is a key aspect of the kinetics that is usually ignored in kinetic analyses based purely on mass action.

In situations where $\gamma$ (and the mechanism) remain constant, $\log(\Re_0)$ is expected to vary linearly with $\log(P_{O_2})$ and $1/RT$, according to the slopes in Table 3. In situations where $\gamma$ varies significantly over a range of data, the expressions for $n$ and/or $E_A^{eff}$ in Table 3 can be reintegrated to predict how $\log(\Re_0)$ will vary nonlinearly with $\log(P_{O_2})$ and $1/RT$.

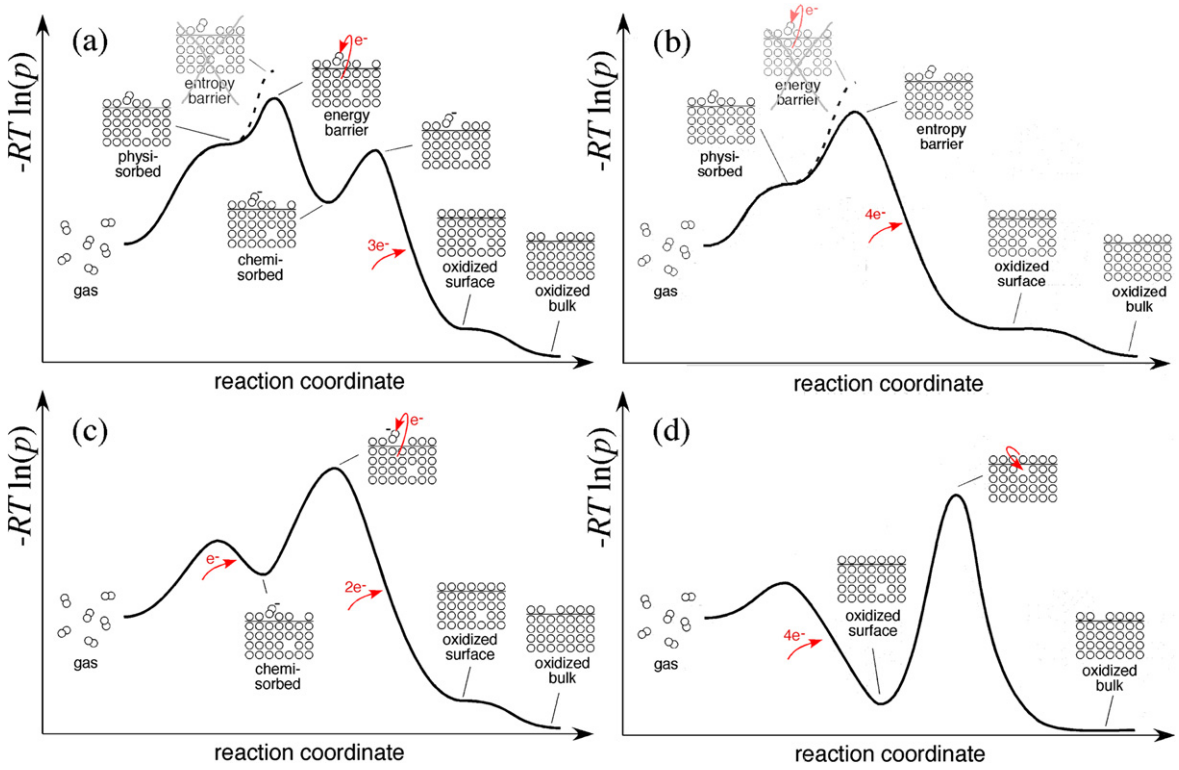


Fig. 5. Qualitative plots of relative probability $p$ (defined in Section 3.3) of various configurations along the reaction coordinate for four scenarios considered in modeling the oxygen exchange rate on $La_{1-x}Sr_xCoO_{3-\delta}$ and $La_{1-x}Sr_xFeO_{3-\delta}$. Increasing values of $-RT\ln(p)$ indicate less probable configurations, such that peaks correspond to possible rate-limiting transitions states. All four scenarios assume that monatomic oxygen at the surface has the same negative charge as bulk oxygen ions. In (a) and (b), the reaction is assumed to involve a highly unstable physisorbed diatomic intermediate. In (a), the reaction is limited by formation of a somewhat more stable chemisorbed diatomic intermediate (superoxide), followed by equilibrated 3-electron reduction ("chemisorption limited"). In (b), the reaction is limited by a low probability of finding a second vacancy near the unstable physisorbed intermediate, whereupon rapid 4-electron reduction occurs ("dissociative adsorption-limited"). Whether (a) or (b) dominates depends on the relative probabilities of $O_2 + e^- \rightarrow O_2^-$ (energy barrier) vs $O_2 + V_{O_s} \rightarrow 2O_{O_s}$ (entropy barrier). In (c), the rate-limiting step is assumed to involve dissociation of superoxide *via* an energy barrier ("dissociation-limited"). In (d), the surface is assumed equilibrated with the gas, and the rate-limiting step is exchange of oxygen vacancies with the bulk ("incorporation limited").

### 3.3. Limiting cases of the kinetics considered for comparison

The remaining parameters influencing $n$ and $E_A^{\text{eff}}$ in Table 3 are related to our assumptions about the kinetics. In what follows, we consider four representative scenarios:

(a) *Chemisorption-limited*. The reaction is assumed to be limited by adsorption [Eq. (5a)], with superoxide $O_2^-$ ($(O_2)'_{O_s}$ in Kröger–Vink notation) as the diatomic intermediate: $q_{\text{ads}} = 1$, $q_{\text{diss}} = 3$. The transition state is assumed to involve an energetic activation barrier to charge transfer, $\Delta H^0_{f,\text{ads}}$, with $\beta_{\text{ads}} = 0.5$ (for a metal) or $\beta_{\text{ads}} = 1$ (for a $p$-type semiconductor).

(b) *Dissociative-adsorption limited*. The reaction is assumed to be limited by dissociation [Eq. (5b)], with physisorbed oxygen as the diatomic intermediate: $q_{\text{ads}} = 0$, $q_{\text{diss}} = 4$. The transition state is assumed to involve no energy barrier ($\Delta H^0_{f,\text{diss}} = 0$), but remains limited by the low probability of an unstable physisorbed molecule interacting with a second surface vacancy before desorption. Because this probability is governed purely by mass action in the forward direction, $\beta_{\text{diss}} = 1$.

(c) *Dissociation-limited*. The reaction is assumed to be dissociation limited [Eq. (5b)], where superoxide dissociation involves an energetic activation barrier ($q_{\text{diss}} = 3$ and $\beta_{\text{diss}} = 0.5$). Note that this does not imply a three-electron reaction, only that the apparent reaction order is 3 in electronic species due to equilibration of downstream steps.

(d) *Incorporation-limited*. The gas is assumed to be equilibrated with the surface, and thus the reaction is limited by exchange of vacancies with the bulk [Eq. (5c)]. Because we have assumed that the oxide surface is fully reduced, $q_{\text{incorp}} = 0$.

Fig. 5 depicts these four scenarios qualitatively in terms of the relative probability $p$ of various configurations along the reaction coordinate. The mathematical definition of $p$ could be any appropriately scaled composition variable (e.g., atom density, partial pressure, mole fraction); however as envisioned here, it is assumed normalized in some way as to be comparable among gas, surface, and bulk species. Thus, increasing values of $-RT\ln(p)$ indicate less probable configurations, and peaks in $-RT\ln(p)$ along the reaction coordinate correspond to transition states. For example, in Fig. 5a, physisorbed $O_2$ is unstable relative to the gas phase due to a negative entropy of adsorption, and thus has a higher values of $-RT\ln(p)$. A physisorbed oxygen adjacent to a second vacancy is even less probable, and thus appears even higher on the $-RT\ln(p)$ scale.

Likewise, an energetic transition state (en route to chemisorbed oxygen) would also be less populated than physisorbed oxygen (Fig. 5b). Given similar pre-exponential factors, the relative rates of chemisorption versus dissociative adsorption would be determined by these bottleneck configurations. In following sections, we compare the calculated exchange rate for these scenarios with measured values for $La_{1-x}Sr_xCoO_{3-\delta}$ (LSC) and $La_{1-x}Sr_xFeO_{3-\delta}$ (LSF).

### 3.4. Comparison to measured oxygen exchange rates on $La_{1-x}Sr_xCoO_{3-\delta}$ (LSC)

The thermodynamic properties of $La_{1-x}Sr_xCoO_{3-\delta}$ (LSC) are reasonably well understood, exhibiting values of $\gamma$ spanning $-1/2$ (for small values of $x$ and $x_v$) to $\sim -0.05$ for heavily doped LSC at the highest temperatures and lowest $P_{O_2}$'s that are stable [50]. Fitting of Eq. (15) to gravimetric and coulometric titration data [50,51] provides the values of $g_0$, $\Delta H^0_{rxn}$, and $\Delta S^0_{rxn}$, as summarized by Lankhorst [9]. From these parameters, $\gamma(T, P_{O_2})$ may be calculated as a function of $\varepsilon$ according to Eq. (26b), and substituted into the expressions for $n$ in Table 3. These expressions also can be integrated to predict how $\log(\Re_0/\Re_0|_{P_{O_2}=1\text{ bar}})$ will vary with $\log(P^{eqb}_{O_2})$.

The results of this calculation, for representative values of $\varepsilon$, are given in Fig. 6 for the each of the scenarios outlined in Fig. 5. These plots illustrate two related observations. First, depending on the scenario, the predicted slope of $\log(\Re_0)$ versus $\log(P_{O_2})$ is generally not a constant, but depends on the range of $P_{O_2}$'s over which data is collected. This may help explain the very wide range of values for $n$ reported by different workers for nominally the same materials [20,49,52–55]. Second, except for case (d), the slopes of different scenarios match each other under certain conditions, making it difficult to determine which scenario (if any) is operative based solely on an average value of $n$ calculated over a particular narrow range of $P_{O_2}$. A better approach is probably to examine $\Re_0$ over a wide range of $x$, $T$, and $P_{O_2}$ so that overall trends can be more clearly seen.

The most complete study to date of equilibrium $O_2$ exchange on LSC versus $x$, $T$, and $P_{O_2}$ has been published by van de Haar and coworkers [49]. With permission from these authors, we have obtained their raw data for $K_{tr}(x, T, P_{O_2})$ (measured by conductivity relaxation), calculated $\Re_0(x, T, P_{O_2})$ according to Eqs. (23)–(24) (assuming $\lambda = 1$ and Lankhorst's model for $x_v$), and normalized to $P_{O_2} = 1$ atm. Resulting data for $x = 0.2$, 0.5, and 0.7 at 750 °C is shown in Fig. 6b. Comparing this data to the scenarios in Fig. 6, it would appear that scenario (b) (dissociative adsorption) is overall the most consistent with the $P_{O_2}$ dependance of the exchange rate. This scenario most closely matches the slope and curvature of the data, including the saturation ($n \to 0$) under conditions of low oxygen vacancy concentration (small $\varepsilon$). Note that this is a theoretical prediction of the exchange rate based on the measured thermodynamics

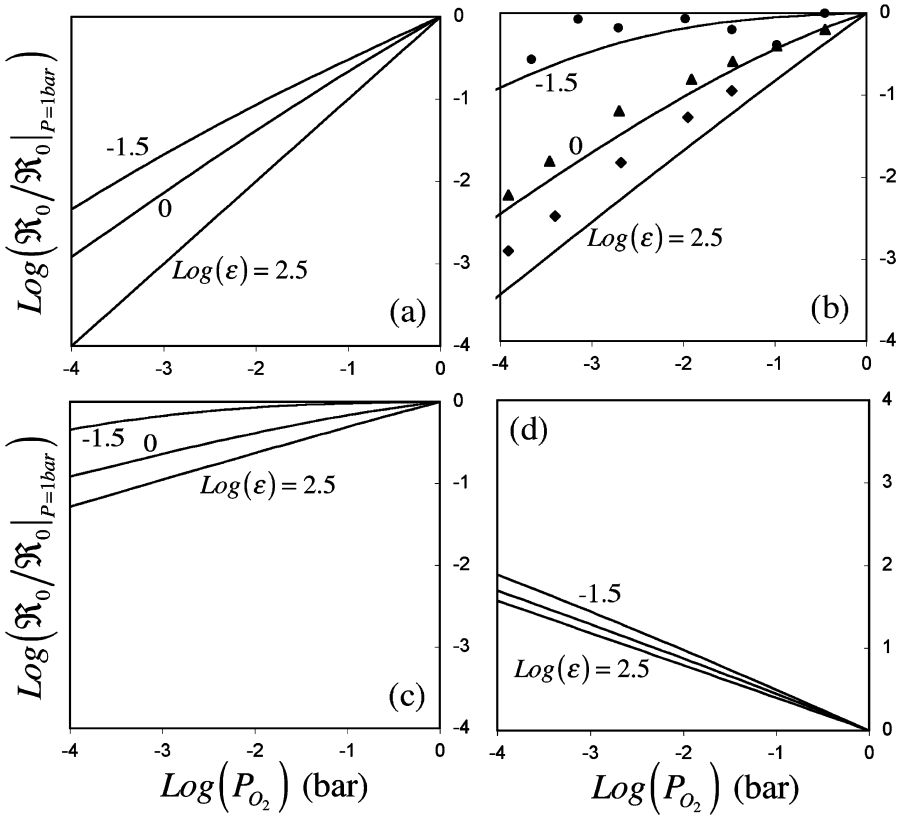


Fig. 6. Theoretical predictions of the equilibrium $O_2$ exchange rate $\Re_0$ of $La_{1-x}Sr_xCoO_{3-\delta}$ vs $\log(P^{eqb}_{O_2})$ and $\log(\varepsilon)$ (as defined in Eq. (26b)) for the four scenarios outlined in Fig. 5: (a) chemisorption limited; (b) dissociative adsorption limited; (c) dissociation limited; and (d) incorporation limited. Data in (b) are experimental values of $\Re_0$ at 750 °C from reference [49], converted to $\Re_0$ from $K_{tr}$ as described in text. Circles, triangles, and diamonds correspond to $x = 0.2$, 0.5, and 0.7. These data represent a range of $\log(\varepsilon)$ of $-1.4$ (for $x = 0.2$) to 2.8 (for $x = 0.7$), as calculated from the nonstoichiometry model.

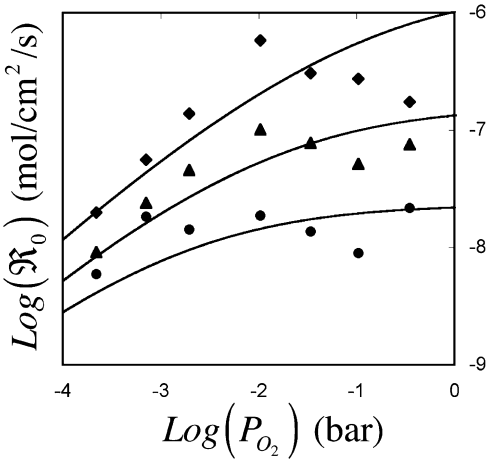


Fig. 7. Measured equilibrium $O_2$ exchange rate $\Re_0$ of $La_{0.8}Sr_{0.2}CoO_{3-\delta}$ vs $\log(P_{O_2})$ and $T$ (from Ref. [49], converted to $\Re_0$ from $K_{tr}$ as described in text). Circles, triangles, and diamonds correspond to $T = 750$, 800, and 850 °C, respectively. These temperatures also correspond to $\log(\varepsilon) = -1.36$, $-1.01$, and $-0.69$, respectively. Simulations for $\log(\varepsilon) = -1.5$, $-1$, and $-0.5$ are shown for comparison.

and the kinetic assumptions in Fig. 5, with no adjustable parameters except magnitude [$\Re_0$ (1 atm)].

Fig. 7 shows the measured exchange rate of LSC-82 ($x = 0.2$) versus $P_{O_2}$ and $T$, along with the predictions of scenario (b) (dissociative adsorption) at similar values of $\log(\varepsilon)$. This calculation involves one independent adjustable parameter: the kinetic rate constant, which shifts the simulations up or down on the logarithmic plot. In the low-$P_{O_2}$ regime, the simulations correctly predict the observed increase in $n$ (slope) with increasing temperature. The simulations are also consistent with the observed reduction in apparent activation energy with decreasing $P_{O_2}$, from an effective activation energy of $E_A^{\text{eff}} \sim 330$ kJ/mol at ~1 atm, decreasing by ~50% at the lowest $P_{O_2}$'s probed. Examining the predictions for scenario (b) from Table 3, we would expect (for $\Delta H_f^0 = 0$ and $\beta_{\text{diss}} = 1$)

$$E_A^{\text{eff}} = \left(-\Delta H_{\text{diss}}^0\right) - \left(-\Delta H_{\text{rxn}}^0 - 2RT\right)(1 + 2\gamma). \tag{30}$$

This predicts a decrease in $E_A^{\text{eff}}$ with decreasing $P_{O_2}$, as $-1/2 \to \gamma \to 0$, in agreement with the observed trend. Although the data are very noisy at high $P_{O_2}$, agreement may begin to break down at the highest values of $P_{O_2}$, where $n$ appears to become somewhat negative. This might suggest the onset of incorporation limitations under conditions of low vacancy concentration, where we predict $\Re_0 \sim P_{O_2}^{-1/2}$ (Fig. 6d).

If our interpretation of the dominant trends discussed above are correct, then oxygen reduction is limited by dissociative adsorption, at least at moderate $P_{O_2}$'s probed by the measurements. If correct, this result shows that even when no energetic barrier exists ($\Delta H_f^0 = 0$), a significant Arrhenius dependence will still occur due to thermodynamics—in this case, the heat of dissociative adsorption. For example, for $x = 0.2$, at the highest $P_{O_2}$'s shown in Fig. 7, $\gamma$ approaches $-1/2$, and Eq. (30) predicts that $E_A^{\text{eff}} \to -\Delta H_{\text{diss}}^0$. Since $E_A^{\text{eff}} \sim 330$ kJ/mol, this implies $\Delta H_{\text{diss}}^0 \sim -330$ kJ/mol, which is similar in value to the total $\Delta H_{\text{rxn}}^0(x)$ at $x = 0.2$ [40]. In other words, most of the enthalpy of the reaction is tied to the dissociation step. This Arrhenius dependence influences the exchange rate through the surface vacancy concentration, which declines sharply with decreasing temperature.

### 3.5. Comparison with equilibrium oxygen-exchange rates on $La_{1-x}Sr_xFeO_{3-\delta}$ (LSF)

To illustrate the difference between a metallic mixed conductor and a $p$-type mixed conductor, we have calculated the expected $T$ and $P_{O_2}$ dependencies of the exchange rate on $La_{1-x}Sr_xFeO_{3-\delta}$ (LSF), an electron-rich $p$-type mixed conductor. We only show results for scenarios (a) and (b) in Fig. 5 because the results for the scenarios (c) and (d) are so far off from measured values. Since charge transfer is limited in this case by hole mass action, we assume $\beta_j = 1$ (as discussed in Section 2.7) for both scenarios (a) and (b).

The oxygen-exchange thermodynamics of LSF are well understood, and have been modeled previously by Mizusaki and coworkers [47]. It is straightforward to convert the parameters of their model to those defined in this paper, thereby providing the functional dependence of $\gamma(x, T, P_{O_2})$. The specific translation is $\Delta G_{\text{rxn}}^0 - 4RT \ln N_{\text{VB}} = 2(\Delta H_{\text{O}} - T\Delta S_{\text{O}})$ [47].

Fig. 8 shows the results of this calculation at representative vales of $\log(\varepsilon)$. The predictions are rather similar to those for LSC, although some subtle differences are present. The chemisorption-limited case generally exhibits a more variable value of $n$, varying between 0.5 and 1 over the range of the simulations. For the dissociative-adsorption case, a saturation of the exchange rate is predicted at increasingly negative values of $\log(\varepsilon)$.

Ten Elshof and coworkers have measured the oxygen-exchange rate on LSF ($x = 0.1$ and 0.4) as a function of $\log(P_{O_2}) = -5.5 \sim 0$ and $T = 650$–$950$ °C [48]. In this case, these authors converted their measurements of the chemical-exchange coefficient "$K_{\text{ex}}$" to an effective isotope-exchange coefficient "$k_0$" (proportional to $\Re_0$). (We have repeated this conversion independently, and agree with it.) In general, their data show that $n$ falls in a much narrower range of values for LSF than LSC, varying from 0.5 to 1 over a similar range of conditions. Fig. 8a shows representative data for LSF over a similar range of $\log(\varepsilon)$ covered by the simulations. In particular, the apparent saturation of $\Re_0$ at low $\varepsilon$ predicted by scenario (b) does not occur in LSF as it did in LSC. Overall agreement is much better for scenario (a) in the case of LSF, suggesting that the rate-limiting step may be chemisorption. This is in general agreement with ten Elshof et al., who posited that the rate-limiting step involved molecular $O_2$ and one vacancy [48].

Another factor consistent with this diagnosis is the effective activation energy. Substitution of Eq. (29b) and $\beta_{\text{ads}} = 1$ into Table 3 reveals that for scenario (a), $\Delta E_A^{\text{eff}}$ should become equal to $\Delta H_{f,\text{ads}}^0 + \Delta H_{\text{incorp}}^0$ in the limit of large $\varepsilon$, which might be smaller than the energy barrier itself ($\Delta H_{f,\text{ads}}^0$) due to a small but possibly negative $\Delta H_{\text{incorp}}^0$. This is consistent with the data, which show a decreasing dependence on $T$ at the highest temperatures [48].

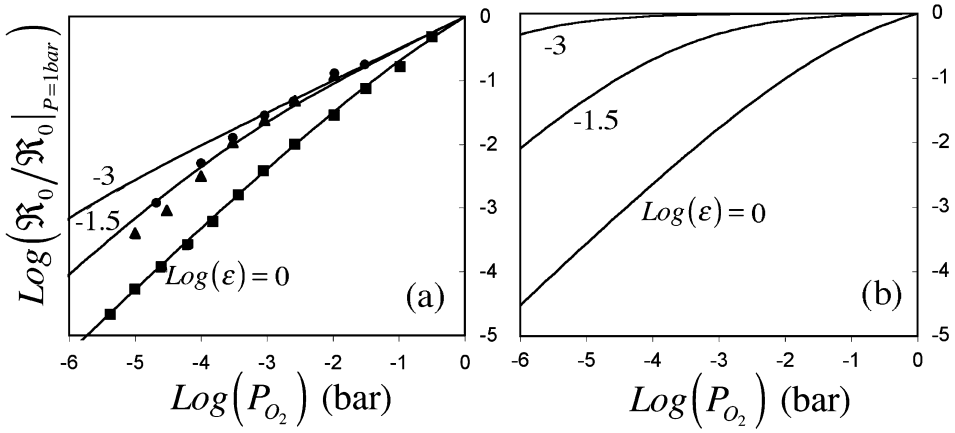


Fig. 8. Theoretical predictions of the equilibrium $O_2$ exchange rate $\Re_0$ of $La_{1-x}Sr_xFeO_{3-\delta}$ (LSF) vs $\log(P_{O_2}^{eqb})$ and $\log(\varepsilon)$ (as defined in Eq. (28b)) for the two scenarios outlined in Figs. 5a and 5b. Data in (a) are normalized experimental values of $k_0$ (proportional to $\Re_0$) from Ref. [48] for $x = 0.1$ at 725 °C (circles), $x = 0.1$ at 875 °C (triangles), and $x = 0.4$ at 950 °C (squares). These three conditions correspond to $\log(\varepsilon) = -3$, $-1.5$, and 0, respectively, as calculated from the nonstoichiometry model.

Why LSF and LSC might differ in mechanism is a subject worthy of speculation. Comparing Figs. 4a and 4b shows that these mechanisms are not radically different, but involve two competitive, possibly parallel pathways. It scenario (a), it is more probable that physisorbed $O_2$ will find another vacancy and dissociate (with no activation energy) rather than cross an activation barrier and become chemisorbed. In scenario (b), the order is reversed; it is more probable that physisorbed $O_2$ will cross an energetic barrier to become stabilized as a chemisorbed intermediate rather than find a second vacancy and dissociate before desorption.

The relative probability of these two competing transition states can be compared mathematically by calculating the transition probabilities for these two competing processes. Let us define $p$ in this case as the equilibrium exchange rate $\Re_0$ (as given in Table 2) divided by the pre-exponential factor, evaluated at $P_{O_2} = 1$ atm. Assuming that the Fermi level contribution to the kinetics is comparable in both scenarios, $\Delta G^0_{\text{incorp}} \sim 0$ (vacancies are equally stable on the surface as in the bulk) and $\Delta G^0_{f,\text{diss}} \sim 0$ (no significant energy barrier for dissociation), we obtain

$$\text{scenario (a):} \quad -RT\ln(p) = \frac{\Delta G^0_{f,\text{ads}}}{RT} + \frac{-\Delta G^0_{\text{rxn}}}{2RT} \tag{31a}$$

and

$$\text{scenario (b):} \quad -RT\ln(p) = \frac{-\Delta G^0_{\text{diss}}}{RT}. \tag{31b}$$

This comparison illustrates the essential difference between these two cases. When chemisorption is rate controlling [Eq. (31a)], the reaction is limited partly by free surface site availability (determined by $\Delta G^0_{\text{rxn}}$) and partly by an energetic barrier to charge transfer ($\Delta G^0_{f,\text{ads}}$). As such, this scenario fits within our traditional view of an activated process (energy barrier). When dissociative adsorption is rate-controlling [Eq. (31b)], the reaction is limited entirely by site availability relative to the physisorbed state ($\Delta G^0_{\text{diss}} = \Delta G^0_{\text{rxn}} - \Delta G^0_{\text{ads}}$). This scenario stands at odds with our traditional view of an activated process, because no energetic barrier is required. It is an "entropy barrier"—a bottleneck to the reaction that involves a highly disfavored (improbable) statistical configuration unrelated to a Boltzmann activation factor.

Because $\Delta G^0_{\text{ads}}$ is expected to be positive, whereas $\Delta G^0_{\text{rxn}}$ is negative, $-\Delta G^0_{\text{diss}}$ decreases as the physisorbed state becomes increasingly stable. Thus if the activation energy for chemisorption is relatively high ($\Delta G^0_{f,\text{ads}}$ is large), and the physisorbed state is relatively stable ($-\Delta G^0_{\text{diss}}$ is low), the barrier to dissociative adsorption will be lower than that for chemisorption (Fig. 5b). In this case, it is more likely that a collision with a second vacancy will occur before the transition to the chemisorbed state. In contrast, if the activation energy for chemisorption is relatively low, and the physisorbed state is relatively unstable ($-\Delta G^0_{\text{diss}}$ is large), chemisorption will control (Fig. 5a).

Based on these considerations, we can speculate that the difference between LSC and LSF may have to do with the metallic band structure of LSC, which would tend to stabilize the physisorbed state. This may serve as a partial explanation for why LSC generally has better initial performance as a solid oxide fuel cell cathode than LSF, particularly on ceria where resistances at the solid–solid interface are small compared with those of zirconia [1]. This may also helps explain the success of the ceria-based fuel cell cathode $La_{0.4}Sr_{0.4}Co_{0.2}Fe_{0.8}O_{3-\delta}$. Perhaps it has sufficient cobalt to create delocalized electronic states at the surface, while remaining generally more thermodynamically stable that LSC. This may also partially explain the very high apparent oxygen exchange rates reported for more recently discovered SOFC cathode materials BSCF and PBCO [56,57], which appear to be very highly conductive metals under SOFC operating conditions.

## 4. Questions for discussion

Reinterpretation of published oxygen exchange rates on mixed conductors using the theory presented in this paper (Section 3) suggest that $O_2$ reduction on electron-rich mixed-conducting oxides is limited by adsorption rather than an energetic barrier to dissociation. This conclusion stands in con-

trast to conventional wisdom, which generally views $O_2$ as a difficult-to-activate molecule. These tentative conclusions are based on limited data involving many uncertainties of procedure, interpretation, and analysis, and thus are far from definitive. However, they raise a number of questions for consideration by other workers and for motivating current and future research.

### *4.1. What is the surface structure, and which reactive intermediates are relevant?*

Published mechanisms for oxygen exchange on mixed conductors (including some proposed by us [25]) often involve unconstrained assumptions regarding surface coverage and the identity of reactive intermediates. Proposed species include $O_2$, $O_2^-$, $O_2^{2-}$, O, $O^-$, and $O^{2-}$, with the degree of surface polarization often left ambiguous; for example, does "$O^-$" bonded to the surface imply charge separation from the bulk, or simply a doubly charged ion where one of the electrons is involved with a bond to the surface? Langmuir adsorption is also usually assumed, implying that under some conditions, species could adsorb noncompetitively on the oxide surface as if it were a metal catalyst under high vacuum. Finally, as discussed in Section 2.7, the implicitly assumed symmetry parameter $\beta$ can acquire an enormous span of values depending on the worker's assumptions about the role of electronic species and the transition state. With so many unconstrained possibilities, multiple explanations for a given set of equilibrium exchange measurements are almost guaranteed.

Examples of this inherent ambiguity are provided in the recent literature. De Souza has summarized the oxygen isotope-exchange properties for a variety of mixed conductors spanning a wide range of electronic transference number [20]. His analysis shows that the $P_{O_2}$ dependence of the oxygen-exchange rate for all the materials can be correlated (within experimental error) to their individual thermodynamic properties using a single empirical relationship,

$$n = \partial \ln \Re_0 / \partial \ln P_{O_2}^{eqb} = 1/4 - \gamma/2, \tag{32}$$

where $\gamma = \partial \ln x_v / \partial \ln P_{O_2}$. For example, dilute $p$-type ion conductors (which have $\gamma = 0$), are generally found to obey $n \sim 0.25$. Likewise, $La_{0.6}Sr_{0.4}Co_{0.2}Fe_{0.8}O_{3-\delta}$ (LSCF), which exhibits $\gamma = -0.32$ under the relevant measurement conditions, is predicted by Eq. (32) to exhibit $n \sim 0.41$, in good agreement with the measured value of $0.39 \pm 0.04$.

At first glance, this correlation might suggest a common mechanism for all materials. Applying mass action kinetics, De Souza examined the possibility that $O_2$ adsorbs dissociatively in low coverage as "O" on the oxide surface, leading to an equilibrium surface coverage proportional to $P_{O_2}^{1/2}$. Assuming that charge transfer between surface and bulk is rate-limiting ("O" $\rightleftharpoons$ "$O^-$"), this leads to an exchange rate that scales as $n = 1/4 - \gamma/2$, in agreement with the observed correlation [20].

But if we apply the theory developed in Section 3 to LSCF, an alternate explanation emerges. If we assume that LSCF is semimetallic and limited by dissociative adsorption, then we would predict $n = 1 + 2\gamma$, which for the same value of $\gamma$ predicts $n = 0.36$, also in agreement with the measured value of $0.39 \pm 0.04$. This comparison raises the possibility that the correlation in Eq. (32) is simply fortuitous, and that the rate-limiting step governing LSCF is different than that for dilute $p$-type materials.

Which of these theories is correct (if any) is difficult to assess without further information. To resolve this degeneracy, one might try to examine the *curvature* (as well as the local slope) of $\ln \Re_0$ vs $\ln P_{O_2}^{eqb}$, but this puts a much more stringent requirement on the range and precision of the data. Whether this approach can really separate all possible scenarios is unclear. In all likelihood, the true mechanism(s) cannot be determined without a more definitive determination of the nonlinear kinetics and incorporation of independent information about the surface structure and relevant reactive intermediates.

### *4.2. Is the reaction limited by an energetic barrier or site availability?*

Conventional wisdom holds that $O_2$ is a difficult molecule to activate energetically, which is why it is so difficult to find an effective electrocatalyst for SOFC cathodes. However, the results in Section 4 call this assertion into question. For electron-carrier-rich materials like LSC and LSF, it appears that dissociative adsorption (without an energy barrier) or chemisorption may be limiting. It is emphasized that barriers to these processes can be partially or wholly entropic (limited by availability of intermediates or sites) rather than energetic. The fact that the exchange rate has a strong Arrhenius dependence cannot be taken as evidence for an activation barrier; a strong Arrhenius dependence is expected even when the reaction is limited by site availability, due to a negative enthalpy of dissociative adsorption.

De Souza and Kilner [58] summarized the kinetic and diffusion properties of various oxide ion conductors and found a strong, general correlation between oxygen-exchange kinetics and bulk oxygen ion transport. This correlation approximates a power law, with $b = \partial \ln k^* / \partial \ln D^*$. However, these authors reported a notable difference in the value of $b$ for electron-carrier-poor versus electron-carrier-rich materials. For electron-carrier-poor materials, $b$ reaches values as high as 3–4. For electron-rich mixed conductors, $b$ falls in a range of 0.5–1. Because the activation energy for diffusion in most ion conductors is similar, the stronger factor influencing $b$ would be the relative Arrhenius dependencies of the kinetics. Thus a reduced value of $b$ for electron-rich materials may represent a change from activation-limited dissociation to adsorption-limited dissociation when electronic states at the Fermi level become plentiful.

### *4.3. What is the reaction rate under moderate to high driving force?*

As discussed in Section 3.1, the uncertainties of experimentation and interpretation of oxygen-exchange data make it very difficult to conclude anything definitively. All conclusions

drawn in this paper are made based on the $P_{O_2}$ and temperature dependencies of the equilibrium exchange rate, which (even if measured and interpreted correctly) is a very insensitive measure of reaction order. The standard procedure for probing reaction orders in chemical kinetics is to operate a differential reactor far from equilibrium, allowing workers to isolate the forward or backward reaction, and probe reaction orders with respect to reactant concentrations. Likewise, in electrochemistry, the determination of Tafel slopes (anodic and cathodic transfer coefficients) can provide information about mechanism and rate-limiting steps. No such well-established methods have been developed for oxygen exchange on mixed conductors, which are usually operated near equilibrium, or as a membrane or electrode where $O_2$ reduction, $O_2$ evolution, bulk and surface transport, and charge transfer to/from other materials are hopelessly convoluted.

To obtain the required information, new methods are needed that can isolate oxygen-exchange rates under moderate to large driving force, where the nonlinear characteristics of Eq. (1) can be probed. In our laboratory, we are currently developing techniques to do this, including nonlinear impedance spectroscopy (NLEIS) of porous and thin-film mixed-conducting electrodes [59]. We hope that the development of this and other methods will prove useful (when combined with other techniques) for probing the mechanism more definitively.

## 5. Conclusion

Despite numerous studies of oxygen exchange and other reactions on the surface of mixed conducting oxides, our fundamental understanding of these reactions remains quite limited. This paper outlines a framework for deriving kinetic rate laws based on proposed reaction mechanisms, applicable to highly defective materials with nonideal thermodynamics. In the case of $O_2$ exchange, we have found that these nonideal thermodynamics play a key role in defining the $P_{O_2}$ and temperature dependencies of the rate law. Comparison of various kinetic scenarios with published oxygen-exchange data for $La_{1-x}Sr_xCoO_{3-\delta}$ (LSC) and $La_{1-x}Sr_xFeO_{3-\delta}$ (LSF) suggest that for electron-carrier-rich mixed conductors, oxygen exchange is governed by chemisorption or dissociative adsorption on limited surface vacancy sites. This conclusion stands in contrast to conventional wisdom, which usually assumes dissociation due to an activation barrier is limiting. Differences in the kinetics between LSC and LSF suggest that metallic band structure may play an important catalytic role by stabilizing physisorbed $O_2$ on the surface. We note that equilibrium exchange rates (as measured using isotope tracers or small-perturbation methods) are inherently ambiguous probes of mechanism, often consistent with numerous possible mechanisms. Additional kinetic data involving moderate to large displacements from equilibrium would be helpful in distinguishing competitive theories regarding the surface.

## Acknowledgments

The authors thank Andre ten Elshof and Henk Verweij for providing (and clarifying questions regarding) some of the data reproduced in this paper. S.B.A. also thanks Roger De Souza, Eric Stuve, and Joachim Maier for helpful discussions and careful readings of early drafts. This work was supported in part by the National Science Foundation (Grants 9353091, 0222002, and 0412076).

## Appendix A. Derivation and explanation of Eq. (1)

### A.1. Nonconfigurational contributions to the free energy

We begin by considering two general states, $A$ and $B$, that are in equilibrium across an interface, as shown in Fig. A.1a,

$$A \rightleftarrows B. \tag{A.1}$$

At equilibrium, we would write

$$\mu_A = \mu_B, \tag{A.2}$$

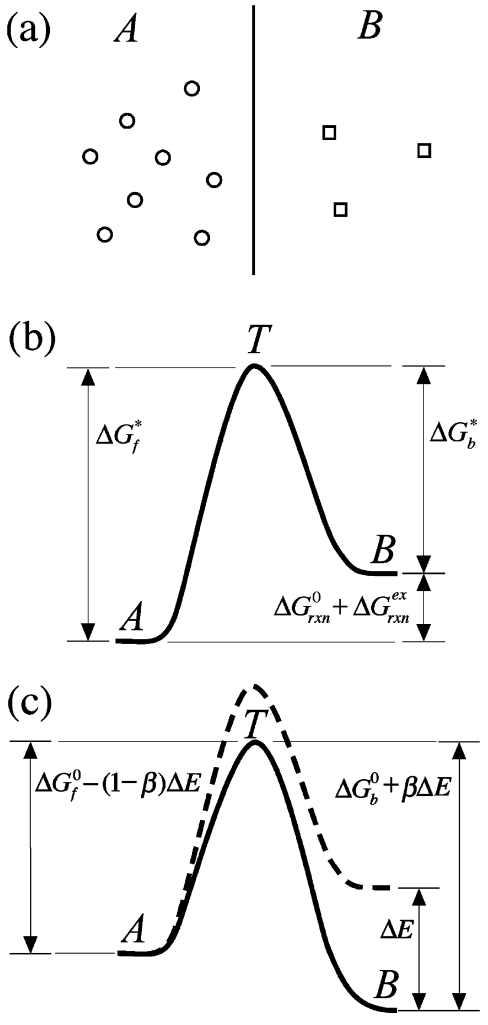


Fig. A.1. (a) Schematic illustrating the transition state pathway for a reaction $A \rightleftarrows B$ across an interface; (b) plot of $G^*$ (defined in Appendix A) along the reaction coordinate; (c) modified energy diagram where $G^*$ of the product is shifted relative to its initial position by $(-\Delta E)$.

where $\mu_i$ is the electrochemical potential of species $i$. We further separate $\mu_i$ into a temperature-dependent reference-state term, $\mu_i^0(T)$, plus a term relating changes in free energy to changes in composition or other nonideal interactions,

$$\mu_A^0 + RT\ln(f_A c_A) = \mu_B^0 + RT\ln(f_B c_B), \tag{A.3}$$

where $f_i$ is the activity coefficient for species $i$. (For changed species, we have adopted Newman's convention where $f_i$ [not $\mu_i^0$] depends on the electrical state [15].) Rearranging Eq. (A.3), we have

$$RT\ln\left(\frac{c_B}{c_A}\right) = -\Delta G_{\text{rxn}}^0 - \Delta G_{\text{rxn}}^{\text{ex}},$$
$$\text{where } \Delta G_{\text{rxn}}^{\text{ex}} = RT\ln\left(\frac{f_B}{f_A}\right). \tag{A.4}$$

Equation (A.4) shows that at equilibrium, the composition (configurational entropy) of the two states will be related through a standard state free-energy difference, $\Delta G_{\text{rxn}}^0 = \mu_B^0 - \mu_A^0$, plus an excess free-energy term, $\Delta G_{\text{rxn}}^{\text{ex}}$, associated with nonideal energetic or entropic interactions, expressible as activity coefficients if desired. For the remainder of this discussion, we consider cases where nonzero $\Delta G_{\text{rxn}}^{\text{ex}}$ is caused either by energetic interactions or the configurational entropic contribution of additional species whose concentrations are tied to the reactants and products.

To examine the consequences of this excess free-energy term $\Delta G_{\text{rxn}}^{\text{ex}}$ on the kinetics, we define $G^*$ as the free energy minus the contribution of configurational entropy of the reacting species along the reaction coordinate. For example, $G^*$ of $A$ would be defined as $\mu_A - RT\ln c_A$, whereas $G^*$ of $T$ might be defined as $\mu_T - RT\ln\Gamma_T$, where $\Gamma_T$ is the interfacial concentration of the transition state in some appropriate set of units. The variation in $G^*$ along the reaction coordinate is illustrated in Fig. A.1b. The transition state (which is mush less probable than the reactant or product) has a higher value of $G^*$ than of $A$ or $B$, differing by $\Delta G_f^*$ and $\Delta G_b^*$, respectively. Applying transition-state theory [13], we expect the kinetics of the reaction $A \rightleftarrows B$ to be governed by the equilibrium population of the transition state ($\Gamma_T$), and thus

$$r = (r_f - r_b) = k\left(c_A e^{-\Delta G_f^*/RT} - c_B e^{-\Delta G_b^*/RT}\right), \tag{A.5}$$

where, to ensure microscopic reversibility, we also have $\Delta G_b^* + (\Delta G_{\text{rxn}}^0 + \Delta G_{\text{rxn}}^{\text{ex}}) = \Delta G_f^*$.

Equation (A.5) shows that even when a system has nonideal thermodynamics, a mass action rate expression can be made consistent with thermodynamics by incorporating nonideal interactions explicitly into the forward and backward rate coefficients $ke^{-\Delta G_f^*/RT}$ and $ke^{-\Delta G_b^*/RT}$. Because in general $\Delta G_f^*$ and $\Delta G_b^*$ may depend on composition and driving force, one must have a specific model for these dependencies to use Eq. (A.5). In chemical kinetics, this model might involve solvent effects, or pressure [16]. In classical electrochemical kinetics, it involves shifts in solution potential [14].

### A.2. Entropic versus energetic driving forces

To better see how Eq. (A.5) fits within the frameworks of chemical and electrochemical kinetics, it is helpful to examine the two asymptotic limits discussed in the Introduction: *entropic* versus *energetic* driving forces. In the entropic limit, the reaction is displaced from equilibrium by altering the *configurational entropy* (composition) of the reactants, but without changing $G^*$ along the reaction coordinate (e.g., $\Delta G_{\text{rxn}}^{\text{ex}} = 0$), and thus $\Delta G_f^* = \Delta G_f^0$ and $\Delta G_b^* = \Delta G_b^0$ are constants. In this case, the thermodynamic driving force, $\Lambda$, may be expressed entirely in terms of displacements in configurational entropy,

$$\Lambda = RT\ln(c_A/c_B) - \Delta G_{\text{rxn}}^0, \tag{A.6}$$

and the rate expression Eq. (A.5) becomes simply

$$r = ke^{-\Delta G_f^0/RT} c_A - ke^{-\Delta G_b^0/RT} c_B, \tag{A.7}$$

which is a simple mass action rate expression having rate coefficients independent of the driving force. This is the type of rate expression applied most often in chemical kinetics and in solid-state systems having thermodynamics that obey point defect theory.

In contrast to an entropic driving force, imagine instead shifting the *energy* of state $B$ relative to state $A$ by an amount $\Delta G_{\text{rxn}}^{\text{ex}} = -\Delta E$, while holding $c_A$ and $c_B$ constant. For example, imagine the energy of $B$ relies on the composition of a third component in the system, and we alter the concentration of that third component. Alternatively, if $B$ is charged, then the energy of state $B$ would depend on an externally applied field. In either case, we would have a modified free-energy diagram relative to the initial equilibrium state, as shown in Fig. A.1c.

As a result of the shift in energy, the free energy of the transition state also may be shifted downward by some amount usually less than or equal to $\Delta E$. Following in the tradition of electrochemical kinetics, we denote this shift as $(1-\beta)\Delta E$, where $\beta$ has a (usually) positive value of order unity, characteristic of the mechanism [14,15]. Recognizing that $\Delta E$ in this case is also equal to the free-energy shift $\Lambda$ of reactants relative to products,

$$\Lambda = \Delta E, \tag{A.8}$$

the rate [Eq. (A.5)] becomes

$$r = ke^{-\Delta G_f^0/RT} e^{((1-\beta)\Lambda)/RT} c_A - ke^{-\Delta G_b^0/RT} e^{-\beta\Lambda/RT} c_B, \tag{A.9}$$

where now the forward and/or backward rate coefficients depend on the thermodynamic driving force $\Lambda$. As we will show below, the value of $\beta$ depends on the nature of the transition state and the degree to which the driving force involves an energetic or entropic displacement from equilibrium.

Maier has previously described the asymptotic cases represented in Eqs. (A.7) and (A.9) as "chemical" and "electrical" experiments, respectively [10]. In what follows, we examine the mixed case, where the driving force involves a generalized displacement from equilibrium.

### A.3. Combined energetic and entropic contributions to the species free energy

A more general free-energy driving force may be defined that incorporates both energetic and entropic displacements from equilibrium, involving both reactants and products. This driving force can be identified by first defining the reactant and product free energies as

$$\mu_A = \mu_A^0 + \varepsilon_A + RT\ln(c_A), \tag{A.10a}$$

$$\mu_B = \mu_B^0 + \varepsilon_B + RT\ln(c_B), \tag{A.10b}$$

where $\varepsilon_i$ is an excess free-energy term associated with nonideal interactions influencing species $i$. We can then define a generalized driving force, $\Lambda = \mu_A - \mu_B$, given by

$$\begin{aligned}\Lambda &= \left(\mu_A^0 - \mu_B^0\right) + (\varepsilon_A - \varepsilon_B) + RT\ln\left(\frac{c_A}{c_B}\right)\\ &= -\Delta G_{\text{rxn}}^0 + \Delta E + RT\ln\left(\frac{c_A}{c_B}\right),\end{aligned} \tag{A.11}$$

where $\Delta G_{\text{rxn}}^0 = (\mu_B^0 - \mu_A^0) + (\varepsilon_B^0 - \varepsilon_A^0)$ is the standard free energy of reaction, defined under conditions where $\Delta G_f^0$ and $\Delta G_b^0$ are also defined, and $\Delta E = (\varepsilon_A - \varepsilon_B) - (\varepsilon_A^0 - \varepsilon_B^0) = -\Delta G_{\text{rxn}}^{\text{ex}}$ is the negative excess free-energy relative to standard conditions. Equation (A.5) then becomes

$$r = kc_A e^{-(\Delta G_f^0 - (1-\beta)\Delta E)/RT} - kc_B e^{-(\Delta G_b^0 + \beta\Delta E)/RT}. \tag{A.12}$$

Recalling that $\Delta G_b^0 = \Delta G_f^0 - \Delta G_{\text{rxn}}^0$, Eq. (A.12) can be reexpressed as

$$r = ke^{-\Delta G_f^0/RT} c_A e^{((1-\beta)\Delta E)/RT}\left[1 - e^{-\Lambda/RT}\right], \tag{A.13}$$

where we have adopted the form of a classical nonequilibrium thermodynamic rate expression, $r = \Re_0[1 - e^{-\Lambda/RT}]$, where $\Lambda$ is the "approach to equilibrium" or "affinity" [60], and $\Re_0$ is a rate prefix that becomes equal to the exchange rate, $r_f = r_b$, in the limit of equilibrium. This expression shows that $\Re_0$ will generally depend on composition, as well as shifts in the energetic contributions to the free energy as a result of applying the driving force.

Equation (A.13) can be generalized to the case with multiple reactants and products, yielding Eq. (1). As shown in Section 3, this further leads to a general prescription for deriving a nonequilibrium rate expression based on a given reaction mechanism. As shown above, this approach requires that we be able to define (or hypothesize) the entropic and energetic contributions to the free energies of the reactants (and reactive intermediates in the case of a multistep reaction). However, the benefit is that thermodynamic consistency is guaranteed from the beginning. In cases where the mechanism dictates $\beta$, this can be incorporated explicitly, usually in terms of mass action. In other cases, $\beta$ can be left as an unknown kinetic parameter subject to experimental determination (as in electrochemical kinetics).

### A.4. Special cases relevant to electrochemical and chemical kinetics

The value of $\beta$ depends on the nature of the transition state. For problems in electrochemical kinetics, where $A$ and $B$ are charged species, the transition state often involves an *energetic barrier*, such as an ion crossing a polarized interface under the influence of an applied field. In this case, we might expect $\beta$ to adopt a fixed fractional value, $0 < \beta < 1$, characteristic of the local fields at the interface [14]. If we also assume that compositions remain fixed, then the driving force becomes purely energetic ($\Delta E = \Lambda$). Defining the overpotential as $\eta = \Lambda/nF$, Eq. (A.13) is usually rearranged as the Butler–Volmer equation [15],

$$\begin{aligned}r = {} & kc_A^{1-\beta} c_B^{\beta} e^{-(\beta\Delta G_b^0 + (1-\beta)\Delta G_f^0)/RT}\\ & \times\left[e^{((1-\beta)nF\eta)/RT} - e^{(-\beta nF\eta)/RT}\right].\end{aligned} \tag{A.14}$$

On the other hand, for problems in chemical kinetics, where deviations from ideality are usually described in terms of specific activity coefficients, Eq. (A.13) can be rearranged as [16]

$$r = k_f\frac{f_A}{f_T}c_A - k_b\frac{f_B}{f_T}c_B, \tag{A.15}$$

where we have defined specific activity coefficients $\Delta G_{\text{rxn}}^{\text{ex}} = RT\ln(f_B/f_A)$ and redefined $\beta$ in relation to the activity coefficient of the transition state, $f_T = f_A^{\beta} f_B^{1-\beta}$, or

$$\beta = \frac{\ln f_T - \ln f_B}{\ln f_A - \ln f_B}. \tag{A.16}$$

Here we expect $\beta$ to be composition-dependent. As recently pointed out by Madon and Iglesia [16], the activity coefficient of the transition state can often share a composition dependency with the reactant or product, leading to a fortuitous cancellation of nonideal effects in the forward or reverse direction, leading to $\beta = 0$ or 1.

A specific case of this situation, relevant to this paper, occurs when the transition state involves an *entropic barrier* (defined as a low-probability event dependent only on composition of the reactants) rather than an energetic barrier. For example, imagine that the reaction involves an additional species, $A + C \rightleftarrows B$, where $C$ is tied in composition to $A$ (by, e.g., site conservation in a lattice, or electroneutrality). Further imagine that the forward rate is governed entirely by the probability of a collision between $A$ and $C$, with no further energetic barriers to formation of $B$ after the collision. In this case, $\Delta G_f^0 = -RT\ln c_C$, a constant independent of the energy of product state $B(\beta = 1)$. Thus Eqs. (A.12)–(A.13) become

$$r = kc_A c_C - ke^{-\Delta G_b^*/RT} e^{-\Lambda/RT} c_B, \tag{A.17a}$$

where the reverse rate coefficient depends (only) on the driving force. Likewise, if the reaction were $A \rightleftarrows B + C$, with the same assumptions applied to the reverse reaction, then we would expect $\beta = 0$, and thus

$$r = ke^{-\Delta G_f^0/RT} e^{\Lambda/RT} c_A - kc_C c_B, \tag{A.17b}$$

where now it is the forward rate coefficients that depends on driving force. In Eqs. (A.17a) and (A.17b), we have identified the specific mass action effect of species C and incorporated it explicitly into the rate expression. Section 3 provides examples in which this approach is (and is not) useful. For semiconducting oxides, it can be helpful to define electrons and holes as explicit species obeying mass action. For metallic mixed conductors, this approach becomes meaningless, because electrons have nominally fixed entropy and ill-defined concentration.

## Appendix B. Selected nomenclature

| Symbol | Units | Meaning | Location |
|---|---|---|---|
| *Roman symbols* | | | |
| $c_0$ | mol/cm$^3$ | oxygen lattice site concentration | Eq. (20) |
| $c_e$, $c_h$ | mol/cm$^3$ | concentration of electrons, electron holes | Eq. (18) |
| $\Delta E_j$ | kJ/mol | shift in standard free energy of reaction associated with a driving force, for reaction step $j$ | Eq. (1) |
| $E_F$ | kJ/mol | Fermi energy relative to core states | Eqs. (9), (18) |
| $E_{\text{gap}}$ | kJ/mol | band gap energy (for a semiconductor) | Eq. (18) |
| $f_i$ | none | activity coefficient of species $i$ | Eq. (A.3) |
| $f_{\text{O}_2}^{\text{solid}}$ | bar | fugacity of $O_2$ in the solid phase | Eq. (14) |
| $\Delta G_{\text{rxn}}^0$ | kJ/mol | standard free energy of reaction | Eq. (A.4) |
| $\Delta G_{\text{rxn}}^{\text{ex}}$ | kJ/mol | excess free energy of reaction | Eq. (A.4) |
| $G^*$ | kJ/mol | total free energy minus configurational entropy | Eq. (A.5) |
| $\Delta G_f^*$, $\Delta G_b^*$ | kJ/mol | free energy barrier for reaction in the forward, backward directions | Eq. (A.5) |
| $\Delta G_j^0$ | kJ/mol | standard free energy of reaction step $j$ | Eq. (13) |
| $\Delta G_{f,j}^0$, $\Delta G_{b,j}^0$ | kJ/mol | unperturbed free energy barrier for reaction step $j$ in the forward, backward directions | Eq. (1) |
| $g_0$ | mol/kJ | density of states at the Fermi level (metal) | Eq. (9) |
| $\Delta H$ | kJ/mol | enthalpy of reaction (see $G$ for super/subscripts) | |
| $k_j$ | various | pre-exponential factor for reaction step $j$ | Eq. (1) |
| $K_{\text{np}}$ | none | electron–hole equilibrium constant (semiconductor) | Eq. (18) |
| $n$ | none | $P_{\text{O}_2}$-exponent of equilibrium oxygen exchange rate | Table 3 |
| $N_{\text{vb}}$, $N_{\text{cb}}$ | mol/cm$^3$ | effective densities of states of valence, conduction band (semiconductor) | Eq. (18) |
| $P_{\text{O}_2}^{\text{gas}}$ | bar | partial pressure of oxygen in the gas | Eq. (14) |
| $q_i$ | none | charge of species $i$ | Eqs. (2), (3) |
| $q_j$ | none | charge transferred during reaction step $j$ | Eqs. (2), (3) |
| $R$ | J/mol K | ideal gas constant (8.314 J/mol/K) | |
| $r_j$ | mol/cm$^2$/s | area-specific rate of reaction step $j$ | Eq. (1) |
| $\Re_{0,j}$ | mol/cm$^2$/s | rate prefix for reaction step $j$ as limiting | Eq. (17) |
| $r_f$, $r_b$ | mol/cm$^2$/s | forward and backward rates of a reaction | Eq. (A.5) |
| $\Delta S$ | J/mol K | entropy of reaction (see $G$ for super/subscripts) | |
| $T$ | K | temperature | |
| $x$ | none | acceptor dopant concentration, e.g. $La_{1-x}Sr_xCoO_{3-\delta}$ | Eq. (8) |
| $x_e$, $x_h$ | none | electron, electron–hole occupancy | Eq. (19) |
| $x_v$ | none | mole fraction of unoccupied oxygen lattice sites | Eq. (6) |
| *Greek symbols* | | | |
| $\beta_j$ | none | reaction symmetry parameter for reaction step $j$ | Eq. (1) |
| $\varepsilon$ | none | dimensionless energy parameter related to nonstoichiometry | Eqs. (26), (28) |
| $\eta$ | volts | reaction overpotential | Eq. (A.14) |
| $\gamma$ | none | thermodynamic factor | Eqs. (26), (28) |
| $\Gamma_i$ | none | surface coverage of species $i$ | Eq. (6) |
| $\lambda_m$ | none | stoichiometric coefficient for reaction step $j = m$ | Eq. (16) |
| $\Lambda$ | kJ/mol | total thermodynamic driving force for the reaction | Eq. (14) |
| $\Lambda_j$ | kJ/mol | thermodynamic driving force for reaction step $j$ | Eq. (1) |
| $\mu_i$ | kJ/mol | electrochemical potential of species $i$ | Eqs. (8)–(11) |
| *Common species and reaction subscripts* | | | |
| $s$ | | surface oxygen vacancy neutral building unit | Eq. (4) |
| $s\text{O}_2$ | | surface diatomic oxygen neutral building unit | Eq. (4) |
| $v$ | | bulk oxygen vacancy neutral building unit | Eq. (4) |
| ads | | of adsorption, or with adsorption as rate-limiting | Eq. (5) |

(*continued on next page*)

Table (*continued*)

| Symbol | Units | Meaning | Location |
|---|---|---|---|
| diss | | of dissociation, or with dissociation as rate-limiting | Eq. (5) |
| incorp | | of incorporation, or with incorporation as rate-limiting | Eq. (5) |
| *Kröger–Vink symbols* | | | |
| O | | oxygen atom | Eq. (2) |
| $O_2$ | | diatomic oxygen | Eq. (2) |
| $V$ | | lattice vacancy | Eq. (2) |
| $()^{\times}$ | | species of neutral charge (relative to un-doped lattice) | Eq. (2) |
| $()^{q\cdot}$ | | species of positive charge $q$ | Eq. (2) |
| $()^{q-}$ | | species of negative charge $q$ | Eq. (2) |
| $()_{O_b}$ | | species located at a normal bulk oxygen lattice site | Eq. (2) |
| $()_{O_s}$ | | species located at a normal surface oxygen lattice site | Eq. (2) |

## References


[1] S.B. Adler, Chem. Rev. 104 (10) (2004) 4791.
[2] S. Diethelm, A. Closset, J. Van Herle, A.J. McEvoy, K. Nisancioglu, Solid State Ionics 135 (1–4) (2000) 613.
[3] R. Bredesen, F. Mertins, T. Norby, Catal. Today 56 (1–3) (2000) 315.
[4] M.H.R. Lankhorst, H.J.M. Bouwmeester, J. Electrochem. Soc. 144 (4) (1997) 1261.
[5] S. Sunde, K. Nisancioglu, T.M. Gur, J. Electrochem. Soc. 143 (11) (1996) 3497.
[6] J.A. Lane, J.A. Kilner, Solid State Ionics 136 (2000) 997.
[7] S. Kim, Y.L. Yang, A.J. Jacobson, B. Abeles, Solid State Ionics 106 (1998) 189.
[8] R.J. Chater, S. Carter, J.A. Kilner, B.C.H. Steele, Solid State Ionics 53–56 (1992) 859.
[9] M.H.R. Lankhorst, H.J.M. Bouwmeester, H. Verweij, Phys. Rev. Lett. 77 (14) (1996) 2989.
[10] J. Maier, Solid State Ionics 112 (3–4) (1998) 197.
[11] J. Maier, Solid State Ionics 135 (1–4) (2000) 575.
[12] J. Maier, Physical Chemistry of Ionic Materials: Ions and Electrons in Solids, Wiley, New York, 2004, p. 538.
[13] M. Boudart, Kinetics of Chemical Processes, Prentice–Hall, Englewood Cliffs, NJ, 1968.
[14] K.J. Vetter, Electrochemical Kinetics, Theoretical and Experimental Aspects, Academic Press, New York, 1967.
[15] J.S. Newman, K.E. Thomas-Alyea, Electrochemical Systems, third ed., Wiley, New York, 2004.
[16] R.J. Madon, E. Iglesia, J. Mol. Catal. A 163 (2000) 189.
[17] E.E. Gonzo, M. Boudart, J. Catal. 52 (1978) 462.
[18] R.J. Madon, J.P. O'Connel, M. Boudart, AIChE J. 24 (1978) 904.
[19] C.A. Eckert, M. Boudart, Chem. Eng. Sci. 18 (1963) 144.
[20] R.A. De Souza, Phys. Chem. Chem. Phys. 8 (7) (2006) 890.
[21] J. Fleig, Phys. Chem. Chem. Phys. 7 (9) (2005) 2027.
[22] D.S. Mebane, M.L. Liu, J. Solid State Electrochem. 10 (8) (2006) 575.
[23] A.M. Svensson, S. Sunde, K. Nisancioglu, J. Electrochem. Soc. 145 (4) (1998) 1390.
[24] A.M. Svensson, S. Sunde, K. Nisancioglu, J. Electrochem. Soc. 144 (8) (1997) 2719.
[25] S.B. Adler, J.A. Lane, B.C.H. Steele, J. Electrochem. Soc. 143 (11) (1996) 3554.
[26] A. Trovarelli, Catal. Rev. Sci. Eng. 38 (1996) 439–520.
[27] J.C. Vedrine, Top. Catal. 21 (1–3) (2002) 97.
[28] H. Over, Y.D. Kim, A.P. Seitsonen, S. Wendt, E. Lundgren, M. Schmid, P. Varga, A. Morgante, G. Ertl, Science 287 (5457) (2000) 1474.
[29] J.C. Vedrine, J.M.M. Millet, J.C. Volta, Catal. Today 32 (1–4) (1996) 115.
[30] M.S. Islam, G. Balducci, Computer Simulation Studies of Ceria-Based Oxides, in: A. Trovarelli (Ed.), Catalysis by Ceria and Related Materials, vol. 2, Imperial College Press, London, 2002, chap. 8.
[31] J. Soria, A. Martinez-Arias, J.M. Coronado, J.C. Conesa, Colloids Surf. A Physicochem. Eng. Aspects 115 (1996) 215.
[32] J.C. Conesa, Surf. Sci. 339 (3) (1995) 337.
[33] J. Soria, A. Martinez-Arias, J.C. Conesa, J. Chem. Soc. Faraday Trans. 91 (11) (1995) 1669.
[34] X.L. Zhang, K.J. Klabunde, Inorg. Chem. 31 (9) (1992) 1706.
[35] H. Idriss, M.A. Barteau, in: B.G. Gates, H. Knözinger (Eds.), Advances in Catalysis, vol. 45, Academic Press, New York, 2000.
[36] T. Kenjo, N. Shiroichi, Electrochim. Acta 42 (23–24) (1997) 3461.
[37] B. Luerßen, J. Janek, R. Imbihl, Solid State Ionics 141 (2001) 701.
[38] M. Nolan, S. Grigoleit, D.C. Sayle, S.C. Parker, G.W. Watson, Surface Sci. 576 (1–3) (2005) 217.
[39] A.R. Allnatt, A.B. Lidiard, Atomic Transport in Solids, Cambridge Univ. Press, Cambridge, UK, 1993.
[40] M.H.R. Lankhorst, H.J.M. Bouwmeester, H. Verweij, J. Solid State Chem. 133 (2) (1997) 555.
[41] B.G. Gates, H. Knözinger, Impact of Surface Science on Catalysis, vol. 45, Academic Press, New York, 2000.
[42] A. Rothschild, Y. Komen, N. Ashkenasy, J. Appl. Phys. 92 (12) (2002) 7090.
[43] G.E. Qingfeng, R. Kose, D.A. King, in: B.G. Gates, H. Knözinger (Eds.), in: Advances in Catalysis, vol. 45, Academic Press, New York, 2000.
[44] G. Etrtl, in: B.G. Gates, H. Knözinger (Eds.), Advances in Catalysis, vol. 45, Academic Press, New York, 2000.
[45] B. Hammer, J.K. Norskøv, in: B.G. Gates, H. Knözinger (Eds.), Advances in Catalysis, vol. 45, Academic Press, New York, 2000.
[46] J. Horiuti, J. Res. Inst. Catal. Hokkaido Univ. 5 (1957) 1.
[47] J. Mizusaki, M. Yoshihiro, S. Yamauchi, K. Fueki, J. Solid State Chem. 58 (1985) 257.
[48] J.E. ten Elshof, M.H.R. Lankhorst, H.J.M. Bouwmeester, J. Electrochem. Soc. 144 (3) (1997) 1060.
[49] L.M. van der Haar, M.W. den Otter, M. Morskate, H.J.M. Bouwmeester, H. Verweij, J. Electrochem. Soc. 149 (3) (2002) J41.
[50] J. Mizusaki, Y. Mima, S. Yamauchi, K. Fueki, H. Tagawa, J. Solid State Chem. 80 (1989) 102.
[51] M.H.R. Lankhorst, H.J.M. Bouwmeester, H. Verweij, Solid State Ionics 96 (1–2) (1997) 21.
[52] R.H.E. van Doorn, I.C. Fullarton, R.A. de Souza, J.A. Kilner, H.J.M. Bouwmeester, A.J. Burggraaf, Solid State Ionics 96 (1997) 1.
[53] M. Sogaard, P.V. Hendriksen, F.W. Poulsen, M. Mogensen, J. Electroceram. 13 (1–3) (2004) 811.
[54] W. Preis, E. Bucher, W. Sitte, J. Power Sources 106 (1–2) (2002) 116.
[55] S. Wang, A. Verma, Y.L. Yang, A.J. Jacobson, B. Abeles, Solid State Ionics 140 (1–2) (2001) 125.
[56] Z.P. Shao, S.M. Haile, Nature 431 (7005) (2004) 170.
[57] G. Kim, S. Wang, A.J. Jacobson, Z. Yuan, W. Donner, C.L. Chen, L. Reimus, P. Brodersen, C.A. Mims, Appl. Phys. Lett. 88 (2) (2006).
[58] R.A. De Souza, J.A. Kilner, Solid State Ionics 126 (1–2) (1999) 153.
[59] J.R. Wilson, D.T. Schwartz, S.B. Adler, Electrochim. Acta 51 (8–9) (2006) 1389.
[60] S.R. De Groot, P. Mazur, Nonequilibrium Thermodynamics, Dover, New York, 1984, p. 544.